Consortium

for

Small-Scale Modelling

Technical Report No. 47

The COSMO Priority Task VAINT: Vegetation Atmosphere INTeractions Report

December 2022

Deutscher Wetterdienst
MeteoSwiss
Ufficio Generale Spazio Aereo e Meteorologia
ΕΘΝΙΚΗ ΜΕΤΕΩΡΟΛΟΓΙΚΗ ΥΠΗΡΕΣΙΑ
Instytut Meteorologii i Gospodarki Wodnej
Administratia Nationala de Meteorologie
ROSHYDROMET
Agenzia Regionale Protezione Ambiente Piemonte
Agenzia Regionale Prevenzione Ambiente Energia Emilia Romagna
Centro Italiano Ricerche Aerospaziali
Amt für GeoInformationswesen der Bundeswehr
Israel Meteorological Service

www.cosmo-model.org

The COSMO Priority Task VAINT: Vegetation Atmosphere INTeractions Report

Evgenii Churiulin[1,2], Merja Toelle[2], Vladimir Kopeikin[3],

Markus Uebel[4], Juergen Helmert[4] and Jean-Marie Bettems[5]

[1] Max Planck Institute for Biogeochemistry, 07745 Jena, Germany

[2] University of Kassel, 34117 Kassel, Germany

[3] Hydrometcenter of Russia, 123242 Moscow, Russia

[4] Deutscher Wetterdienst, 63067 Offenbach am Main, Germany

[5] Federal Office of Meteorology and Climatology, Zurich, CH-8058, Switzerland

Contents

1   Abstract

The COSMO Priority Task: Vegetation Atmosphere INTeractions (**VAINT**) focussed on
the improvement of the vegetation algorithm of the regional climate model COSMO-CLM
v6.0 (v5.16) developing both the impementation new stomatal resistance, leaf photosynthe-
sis, two-big leaf, leaf area index algorithms and the postprocessing instruments. The aim
of the PT VAINT was to improve the vegetation algorithm of COSMO-CLM v6.0 (v5.16)
which is based on the simple resistance Jarvis approach with the BATS model parameteriza-
tion scheme and does not take into account the stomatal regulation and vegetation growth
depending on atmospheric CO_2 concentrations especially relevant in the context of global
warming. The research and development work covered three main areas:

- development and implementation of the new vegetation algorithms into TERRA-ML
  and COSMO-CLM;

- evaluation of the output COSMO-CLM parameters;

- adaptation of the new algorithms for further updates and developments;

2   Introduction

Land surface processes significantly affect the conditions in the low-level atmosphere (Betts
et al., 1996). The surface radiation budget and turbulent heat fluxes are controlled by near-
surface atmospheric conditions. Both determine the amount of energy and water available
for heating and moistening the air over land (Regenass et al., 2021). Further parameters
that determine the interactions between the land surface and atmosphere are the soil water
content (Koster et al., 2002) and the surface roughness (Schaer et al. 2004; de Noblet-
Ducoudre and Pitman, 2021). The impact of surface processes on the air temperature,
humidity, the structure of the planetary boundary layer and precipitation is evident (Arora,
2002). Toelle et al. (2014) have shown in climate simulations at a convection-permitting scale
that vegetation type changes can greatly affect extreme temperatures and evapotranspiration
(ET), which is an important process in the energy and water cycle that links atmospheric and
land surface processes and acts as one of the key components in the energy balance equation
(Dokuchaev, 1899). ET rates depend on numerous local and seasonal biophysical factors
(e.q. leaf area index (LAI) and photosynthesis rate (A)), vulnerable to climate change.

Evapotranspiration simulated by the multilayer land surface scheme TERRA-ML of the
Consortium for Small-scale Modeling (COSMO) was found to be systematically underesti-
mated based on the averaged diurnal cycle of ET over Europe during the growing season for
the vegetated land surface (Schulz et al., 2015; Shrestha and Simmers, 2019). One of the
possible reasons of ET underestimation is that transpiration in TERRA-ML is calculated
with inaccuracy due to the simplified stomatal resistance parameterisation scheme. Also, in
TERRA-ML plants cannot have a different (canopy) temperature than the ground and the
incoming solar radiation is directly used to heat the ground because there is no shading ex-
erted by the vegetation insulating the ground against the solar radiation (Schulz and Vogel,
2020). Detailed information regarding the estimation of evapotranspiration in TERRA-ML
is presented in the work of Regenass et al. (2021).

Plant transpiration is an important parameter, which is coupled with the carbon and wa-
ter cycles and acts as principal feedback between the land surface and atmosphere. Plant
transpiration rates are partly controlled by stomatal conductance (resistance) depending on

environmental, biophysical, and soil water conditions. Changes in CO_2 concentration also effect the leaves response to external influence (Uebel, 2015). Plants are able to balance the uptake of CO_2 required for photosynthesis with the need to maintain sufficient moisture levels inside the leaf (Matheny et al., 2014). Leaves close (low light level, cold temperature, high CO_2 volume, low leaf nitrogen, dry leaf and air) and open (high light level, warm temperature, moderate CO_2 volume, high leaf nitrogen, moist leaf and air) their stomata to regulate dynamically water loss and C uptake (Ball, 1988) and avoid decreases in leaf water potential that could lead to desiccation or catastrophic cavitation within the xylem system (Davin et al., 2011). The increase in global and regional temperatures and potential rise of the variation in regional precipitation creates the necessity for more accurate prediction of stomatal conductance (resistance) depending on heat, water and carbon exchange (Berry et al., 2010; Wu et al., 2012; Jasechko et., 2013).

The current parameterisation scheme of TERRA-ML of COSMO-CLM for stomatal conductance does not take into account the stomatal regulation and vegetation growth depending on atmospheric CO_2 concentrations and uses the phenomenological Jarvis approach based on empirical dependencies between canopy resistance (r_{can}) and environmental variables. Moreover, LAI does not respond to water stress, and depends on vegetation parameters only. Also, COSMO-CLM applies the one-big-leaf approach for radiation fluxes, although this approach has disadvantages that are related to the impossibility of accounting for the difference of the physiological properties between sunlit and shaded leaves (Dai et al., 2004), and overestimation of the reduction of photosynthesis when clouds attenuate solar radiation (Uebel, 2015). In order to overcome these limitations, we decided to substitute the empirical Jarvis approach with the physically based Ball-Berry (Ball and Berry, 1991) approach coupling with leaf photosynthesis processes (Farquhar et al. 1980; Collatz et al., 1991) and introduced a two-big leaf canopy (Thornton and Zimmermann, 2007).

3 Models description

In our research, we were guided by the ideas and published materials (e.g., documentations and model codes) of several existing dynamic vegetation models such as the Community Land Model (Oleson et al., 2010; Oleson et al., 2013), SURFEX (Le Moigne, 2018), and CHTESSEL (Nogueira et al., 2020). Special attention was paid to the successful examples of the CLM implementation into different regional climate models, for example, into the WRF model (Van Den Broeke et al., 2017) or into COSMO-CLM (Davin et al., 2011; Davin and Seneviratne, 2012). Davin et al. (2011) have coupled COSMO-CLM with CLM and found improvements with respect to land surface fluxes, including an improved magnitude of radiation fluxes and a better partitioning of turbulent fluxes, but TERRA-ML used in COSMO-CLM was fully replaced in $COSMO - CLM^2$ with the CLM3.5 parameterisation scheme. The $COSMO - CLM^2$ was created and tested, but Davin et al. (2011) did not perform convection-permitting scale simulations due to high computational costs (Stoeckli et al., 2008). All our improvements have been directly implemented in TERRA-ML of COSMO-CLM, allowing us to improve TERRA-ML and save all the advantages of COSMO-CLM (for example, convection-permitting scale). These changes distinguish our research from the previous research for coupling the COSMO-CLM and CLM models.

3.1 Community Land Model

Community Land Model (CLM) model is a community-developed land surface model maintained at NCAR (National Centre for Atmospheric Research) and includes options for mech-

anistic descriptions of soil physical and vegetation biophysical and biochemical processes. CLM is a single-column soil-snow-vegetation biophysical model. It was designed by combining the best features of three land surface models: the NCAR Land Surface Model (LSM) of Bonan (1996), the Biosphere-Atmosphere Transfer Scheme ($BATS$) of Dickinson et al., (1993) and the Institute of Atmospheric Physics, Chinese Academy of Sciences land model ($IAP94$) of Dai and Zeng, (1997). It is a very modular land surface model that can be applied from regional to global scale and from daily to decadal timescales.

CLM model can be used with a fully prognostic treatment of the terrestrial carbon and nitrogen cycles including interactions between these cycles as mediated by biological mechanisms of plants and soil heterotrophs and mechanistic parameterizations of large-scale vegetation processes in order to dynamically simulate the distribution and structure of natural vegetation (Thornton and Zimmermann, 2007). The CLM model includes parameterization schemes of physical, biophysical, and biogeochemical processes that simulate the terrestrial radiation, heat, water, and carbon fluxes in response to climatic forcing (Stoeckli et al., 2008). The CLM model consists of one vegetation layer, 5 snow layers (if a snowpack exists) and 10 unevenly spaced vertical soil layers characterizing the shallow soil in the upper 3.43 m. Spatial land surface heterogeneity is represented as a nested subgrid hierarchy. Each model grid cell (Fig.1) can incorporate multiple land units, each landunit can consist of different columns and each column can have multiple plant functional types (PFTs). The 16 PFTs (Bonan and Levis, 2002) of CLM differ in plant physiology and structure and capture the biogeophysical and biogeochemical properties of different plant species in terms of their functional characteristics. The current landunits are: *glacier, lake, wet-land, urban and vegetated* (Oleson et al., 2010). The column level handles the variability in the soil and snow state variables within a single landunit. The soil thermal and hydraulic parameters are derived from depth-varying sand and clay percentages using the relations of (Clapp and Hornberger, 1978).
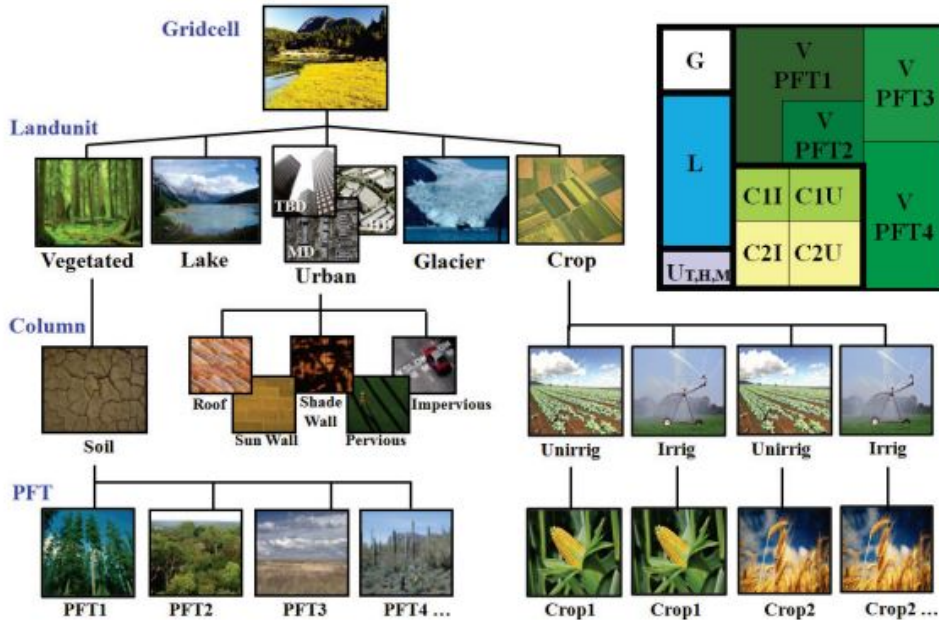

Figure 1: Configuration of the CLM subgrid hierarchy (Oleson et al., 2013)

The physical and biophysical soil and vegetation processes are parameterized. Surface and

canopy albedo is calculated using a two-stream radiative transfer model. The fluxes of momentum, sensible heat and water vapor between the canopy top and the atmosphere are derived from the Monin-Obukhov similarity theory. Turbulent eddy fluxes within the canopy and between the canopy and the ground are represented as a pathway from the ground to the atmosphere using characteristic conductances that are multiplied with the quantity differences. The parameterization of canopy transpiration and canopy evaporation is adopted from BATS and a simple parameterization of ground evaporation is included in CLM. In our research, we used the open-source code of CLMv3.5 (`https://www.earthsystemgrid.org`) and the official documentations (CLMv3.5 (Oleson et al., 2010) and CLMv4.5 (Oleson et al., 2013)) as an example of successful implementation of the Ball-Berry approach coupling with leaf photosynthesis and two-big leaf canopy.

3.2 SURFEX model

The SURFace EXternalisee (*SURFEX*) is a model of the Centre National de Recherches Meteorologiques (CNRM hereafter) and Meteo-France using for better simulating the exchanges of energy and water between the land surface and the atmosphere. The SURFEX model has several land surface parameterisation schemes for example ISBA (Mahfouf and Noilhan, 1996), ISBA-A-gs (Calvet et al., 1998) and special version applying for climate modeling ISBA-CC (Gibelin et al., 2008). The schemes ISBA and ISBA-A-gs computes the exchanges of energy and water between the continuum soil-vegetation-snow and the atmosphere above. The evapotranspiration of the vegetation in ISBA scheme is controlled by a resistance like proposed by Jarvis (1976). However, the ISBA-A-gs accounts for a simplified photosynthesis model where the evaporation is controlled by the aperture of the stomates, the component of the leaves that regulates the balance between the transpiration and the assimilation of CO_2. Both land surface schemes are used in the French operational and research forecast models, that allows us to find a solution how we can implement in COSMO-CLM algorithm for calculations of changes in LAI depending on biomass evolution without a long spin up, because of that we focused our attention on the ISBA-A-gs land surface model.

ISBA-A-gs is able to simulate the diurnal cycle of carbon and water vapor fluxes (Calvet et al., 2008) and can reproduce daily values of LAI and biomass depending on leaf photosynthesis and CO_2 concentrations. ISBA-A-gs calculates interactively the leaf biomass and the LAI (defined as the leaf area per unit ground area), using a growth model. The leaf biomass is supplied with the carbon assimilated by photosynthesis, and decreased by a turnover and respiration terms. However, ISBA-A-gs uses the model of Goudriaan et al. (1985) modified by Jacobs (1994) for calculation of leaf photosynthesis and stomatal resistance. This parameterization is less detailed than that used in most LSM (Calvet et al., 1998). Due to we used only the LAI algorithm from SURFEX in our research and udapted this algorithm for Ball-Berry stomatal resistance approach and Farquhar leaf photosynthesis model.

3.3 COSMO-CLM

The COSMO-CLM is a climatic version (Rockel et al., 2008) of a nonhydrostatic limited area atmospheric prediction model of the Consortium for Small-Scale Modelling (COSMO, `https://www.cosmo-model.org/`). It was developed in Deutscher Wetterdienst, (DWD, `https://www.dwd.de/`). The main purpose of the regional version of COSMO-CLM is weather prediction and various scientific applications on **meso-γ** and **meso-β** scales. The model has a system of horizontal (rotated) and vertical (terrain-following height) coordinates (Doms et al., 2018). The core of COSMO model is the numerical solution of the primitive

thermo-hydrodynamic equations describing fully compressible flow in a moist atmosphere:

$$\rho \frac{d\nu}{dt} = -\nabla p + \rho g - 2\Omega * (\rho\nu) - \nabla(\underline{T}) \tag{1a}$$

$$\frac{dp}{dt} = -(c_{pd}/c_{vd}) \, p\nabla\nu + (c_{pd}/c_{vd} - 1) \, Q_h \tag{1b}$$

$$\rho c_{pd} \frac{dT}{dt} = \frac{dp}{dt} + Q_h \tag{1c}$$

$$\rho \frac{dq^v}{dt} = -\nabla F^v - \left(I^l + I^f\right) \tag{1d}$$

$$\rho \frac{dq^{l,f}}{dt} = -\nabla\left(P^{l,f} + F^{l,f}\right) + I^{l,f} \tag{1e}$$

$$\rho = p \left[R_d \left(1 + (R_v/R_d - 1) \, q^v - q^l - g^f\right) T\right]^{-1} \tag{1f}$$

where: ρ is air density; g and Ω are acceleration of gravity and angular velocity ot the earth; C_P and C_V are specific heat and volume at constant pressure; R_L is gas constant of dry air; T_{virt} is virtual temperature. The model equations are numerically solved using the finite differences method on a rotated spherical grid (Arakawa and Lamb, 1977) arising from the usual geographical coordinate system by a displacement of the model north pole. This displacement is performed in such a way that the model equator is located in the model domain of interest to minimize the convergence of the meridians. In the vertical, a time-independent generalized terrain-following stretched grid of 50 model layers is used with a vertical grid spacing increasing with height. Caused by the compressibility of the non-hydrostatic COSMO, sound waves and high frequency gravity waves are parts of the solution of the system of equations. To avoid numerical instabilities or, alternatively, a very short integration time step, a time-splitting method is applied in the Runge-Kutta integration scheme (Wicker and Skamarock 2002). The precipitation parameterizations scheme uses a one-moment microphysics scheme for five categories of hydrometeors: *cloud, rain, snow, ice* and *graupel*. The radiative transfer scheme (Ritter and Geleyn, 1992) is also applied in COSMO-CLM.

The surface and soil processes are calculated in the multi-layer soil model TERRA-ML (Schrodin and Heise, 2002; Doms et al., 2018), consisting of the two parts. The first one considers hydrological processes including snow melting and freezing. The second one includes algorithms intended for calculations of bare soil evaporation and plant transpiration. In TERRA-ML, we used ten (up to 15.34 m depth) and eight (up to 3.82 m depths) active layers for energy and water transport calculations. TERRA-ML parameterizes all surface fluxes at a grid element and sums them up into a total moisture flux - *evapotranspiration*:

$$(F_{q^v}^3)_{sfc} = -\rho C_q^d |V_h|(q^V - q_{sfc}^V) \tag{2}$$

where: C_q^d is bulk-aerodynamical coefficient for turbulent moisture transfer at the surface; q^V and q_{sfc}^V are specific humidity at the lowest grid level above the ground and ground level, respectively; V_h is absolute wind speed at the surface.

$$-(F_{q^v}^3)_{sfc} = E_b + \sum_{k=1}^{ke_{soil,hy}} T_r + E_i + E_{snow} \tag{3}$$

where: E_b is bare soil evaporation; E_i and E_{snow} are evaporation from the interception and snow, respectively; T_r is plant transpiration. We focused on plant transpiration and didn't change parts of TERRA-ML which are related to hydrological processes, evaporation from bare soil, snow and interception. Plant transpiration is not considered for *ice* and *rock* soil

types. For other soil types, the calculations are based on the $BATS$ scheme if $E_{pot}(T_{sfc}) < 0$:

$$Tr = f_{plant}\,(1 - f_i)\,(1 - f_{snow})\,E_{pot}(T_{sfc})r_a\,(r_a + r_f)^{-1} \tag{4}$$

where: T_r is plant transpiration; r_a and r_f are atmospheric and foliage resistance; f_{plnt}, f_i and f_{snow} are fractional area covered by plants, interception water and snow; $E_{pot}(T_{sfc})$ is potential evapotranspiration. Foliage resistance is related to leaf area index and describes the reduction of transpiration by stomatal resistance (r_s).

$$
\begin{aligned}
r_a^{-1} &= C_q^d|V_h| = C_a & r_f^{-1} &= r'C_F = C_v \\
C_F &= f_{LAI} * r_{la}^{-1} & r_{la}^{-1} &= C'u_*^{0.5} & r' &= r_{la}\,(r_{la} + r_s)^{-1}
\end{aligned}
\tag{5}
$$

where: r' - is resistance describes the reduction of transpiration by stomatal resistance r_s; f_{LAI} is LAI; u_* is frictional velocity; C_A and C_V are transfer coefficients corresponding by the atmospheric and foliage resistance. If we replace the resistances r_a and r_f by the corresponding transfer coefficients C_A and C_V we arrive at the following formula for the total transpiration rate T_r:

$$Tr = f_{plant}\,(1 - f_i)\,(1 - f_{snow})\,E_{pot}(T_{sfc})C_V\,(C_A + C_V)^{-1} \tag{6}$$

The detailed formulation of stomatal resistance in the reference version of COSMO-CLM and new formulation are provided below.

4   Stomatal resistance

In botany, a stoma (plural "stomata") is a pore, found in the epidermis of leaves, stems, and other organs, that controls the rate of gas exchange. Stomatal resistance is an important variable in evaluating plant physiological response to the physical and biological environment. Typical values of r_s for grass are in range from $100\ s\ m^{-1}$ (stoma open) to $5000\ s\ m^{-1}$ (stoma closed). Plants are able to balance the uptake of CO_2 required for photosynthesis with the need to maintain sufficient moisture levels inside the leaf. Kaufmann and Thor, (1982) concluded that water stress, temperature, and wind speed only affect r_s sporadically on plants growing in their natural habitat. Monteith and Unsworth (1990) pointed out that r_s of leaves in their natural environment depended on solar radiation. Solar radiation has a strong influence on the stomatal opening and decreases until light saturation is reached.
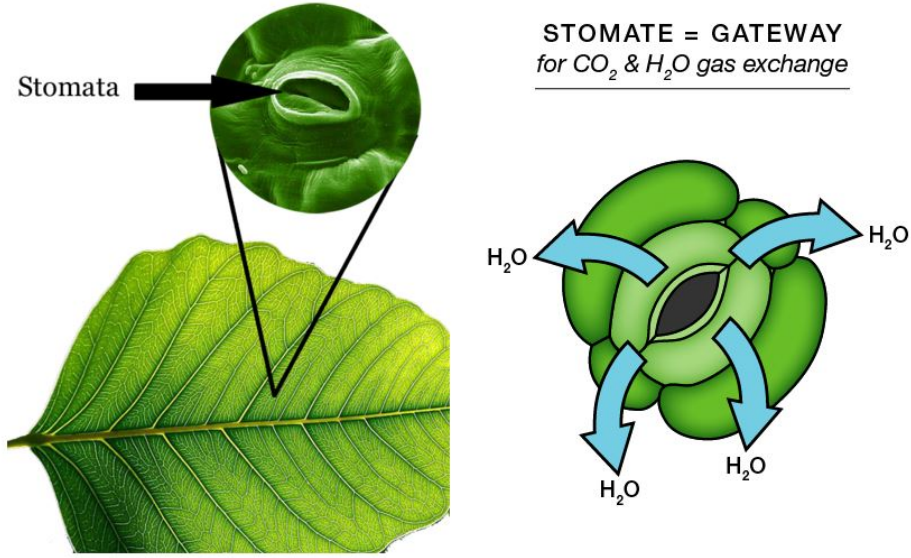
Figure 2: Stomata structure according to (https://www.greencastonline.com/)

Jarvis and Davies (1998) showed that increases in the net rate of photosynthesis are a result of transient increases in the ambient CO_2 concentration, and the reverse is also the case. Moreover, Jarvis (1976) presented a multiplicative and simple resistance model in which resistance was estimated as a function of environmental variables, soil moisture and plant water status. This approach is used in COSMO-CLM model.

4.1 Original version

Stomatal resistance computations are based on the Jarvis approach with the BATS model parameterisation. The approach based on empirical relations between r_s and environmental variables using statistical relationships to determine the model parameters from measurements for different plant types. Thus, with the Jarvis approach r_s is predicted diagnostically depending on functions of solar radiation (Eq.8), atmospheric specific humidity (Eq.9), temperature at a reference height (Eq.10), and soil water availability (Eq.11). Each of these functions are assumed to be independent of each other. Moreover, the influence of atmospheric CO_2 concentration on r_{can} is not considered.

$$r_s^{-1} = r_{max}^{-1} + \left(r_{min}^{-1} - r_{max}^{-1}\right)\left[F_{rad}F_{wat}F_{tem}F_{hum}\right] \tag{7}$$

where: r_{max} and r_{min} are maximal (4000 $s\ m^{-1}$) and minimal (150 $s\ m^{-1}$) values of stomatal resistance. The functions F describe the influence on the stomatal resistance of radiation (F_{rad}), soil water content (F_{wat}), ambient temperature (F_{tem}), and ambient specific humidity (F_{hum}), respectively. These functions take the values from one (optimum conditions) to zero (unfavorable conditions).

$$F_{rad} = min\left(1; \frac{PAR}{PAR_{crit}}\right) \tag{8}$$

where: PAR is photosynthetically active radiation; PAR_{crit} is tuning parameter, which is equal to 100 $w\ m^{-2}$.

$$F_{hum} = 1 - min\left[1; max\left(0; 4\left(\frac{\Delta q}{q_{sat}}\right) - FR_{sat}\right)\right] \tag{9}$$

where: FR_{sat} is tuning parameter equal to 0.75. In the actual version of TERRA-ML the ambient specific humidity equal to one.

$$F_{tem} = max\left[0; min\left(1; 4\frac{(T_{2m} - T_0)(T_{end} - T_{2m})}{(T_{end} - T_0)^2}\right)\right] \qquad (10)$$

where: T_{2m} is temperature in 2m above the soil surface; T_{end} is tuning parameter equal to 315K; T_0 is melting point of water in K (273K).

$$F_{wat} = max\left[0; min\left(1; \frac{w_{l,root} - w_{PWP}}{w_{TLP} - w_{PWP}}\right)\right] \qquad (11)$$

where: $w_{l,root}$ is water content of the soil averaged over the root depth (Eq.12); w_{PWP} and w_{TLP} are permanent wilting point and turgor loss point:

$$w_{l,root} = \frac{1}{z_{root}}\int_{z=0}^{z=z_{root}} w_l(z)dz \qquad (12)$$

$$w_{TLP} = w_{PWP} + (w_{FC} - w_{PWP}) * (0.81 + 0.121\ arctg\left(E_{pot}\left(T_{sfc}\right) - E_{pot,norm}\right)) \qquad (13)$$

where: w_{FC} is water content at field capacity; $E_{pot,norm} = 4.75$.

4.2 Updated version

The new calculations of stomatal resistance (Eq.14) in TERRA-ML are based on the plant physiological Ball-Berry approach (Ball et al, 1987), with algorithms for canopy fluxes based on the Collatz model (Collatz et al., 1991) and improved by Thornton and Zimmermann (2007) through the implementation of a new parameterisation scheme for the maximum rate of carboxylation ($V_{c,max}$), which is presented in (Eq.27). The main assumption of the Collatz model is that r_s depends on the environmental conditions and net leaf photosynthesis, scaled by relative humidity and CO_2 concentration.

$$\frac{1}{r_s} = m\frac{A}{c_s}\frac{e_s}{e_i}P_{atm} + F_{wat}b \qquad (14)$$

where: m is plant functional type (PFT) dependent parameter; A is leaf photosynthesis; c_s and e_s are CO_2 partial pressure and vapor pressure at the leaf surface; e_i is saturation vapor pressure inside the leaf at the vegetation temperature; P_{atm} is atmospheric pressure; b is minimum stomatal conductance when $A = 0$. It should be noted that resistance is converted from units of $s\ m^{-2}\mu mol^{-1}$ to $s\ m^{-1}$ as:

$$1s\ m^{-1} = 1 * 10^{-9}R_{gas}\frac{\theta_{atm}}{P_{atm}} \qquad (15)$$

where: R_{gas} is universal gas constant; θ_{atm} is atmospheric potential air temperature. Canopy resistances for leaf photosynthesis and transpiration at the canopy scale described with a two-big-leaf canopy integration scheme. Using LAI values for sunlit (L^{sun}) and shaded (L^{sha}) leaves, the canopy resistances (sunlit - r_{can}^{sun}, shaded - r_{can}^{sha}) can be derived similarly as for the one-big-leaf assumption:

$$\frac{r_{can}^{sun}}{L^{sun}} = \frac{r_{st}^{sun}}{L^{sun}} + \frac{r_b^{sun}}{L^{sun}}, \qquad \frac{r_{can}^{sha}}{L^{sha}} = \frac{r_{st}^{sha}}{L^{sha}} + \frac{r_b^{sha}}{L^{sha}} \qquad (16)$$

The whole canopy resistance r_{can} (or canopy conductance g_{can}) which governs the water and CO_2 exchange between the foliage and the canopy air can be interpreted as both resistances (r_{can}^{sun} and r_{can}^{sha}) acting in parallel and are scaled by L^{sun} and L^{sha}:

$$g_{can} = \frac{1}{r_{can}} = \frac{L^{sun}}{r_{can}^{sun}} + \frac{L^{sha}}{r_{can}^{sha}} \qquad (17)$$

5 Leaf photosyntesis

Photosynthesis is the process by which green plants and certain other organisms transform light energy into chemical energy. During photosynthesis in green plants, light energy is captured and used to convert water, carbon dioxide, and minerals into oxygen and energy-rich organic compounds. Photosynthesis occurs in chloroplasts within the leaf cells and is the process by which carbohydrates are produced from CO_2 and water H_2O using light energy that is absorbed by the green leaves.

$$nCO_2 + 2nH_2O \overset{PAR}{\rightarrow} CH_2O_n + nO_2 + nH_2O \tag{18}$$
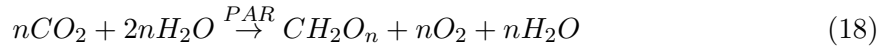
where: n is the number of molecules of CO_2 that combine with H_2O to form carbohydrates. The complement of photosynthesis is respiration which produces energy needed to maintain plant functions (maintenance respiration) and to grow new plant tissues (growth respiration). For this energy production the organic compounds (e.g. glucose $C_6H_{12}O_6$) are oxidized and the chemical reaction of respiration can be formulated as:

$$C_6H_{12}O_6 + 6O_2 \longrightarrow 6CO_2 + 6H_2O \tag{19}$$
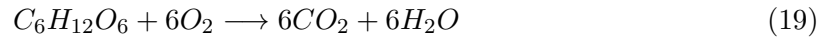
About 50% of CO_2 absorbed in photosynthesis process is released again by plant respiration (Ryan, 1991).
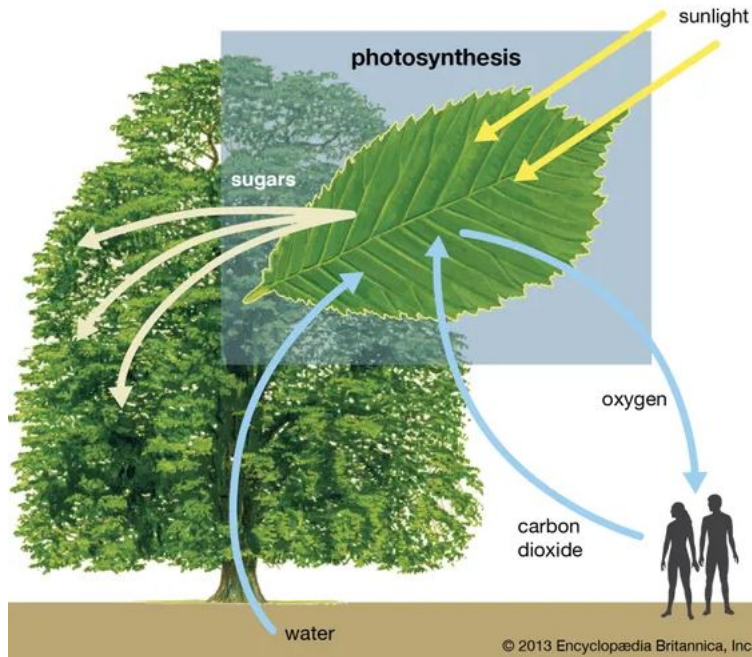
Figure 3: Diagram of photosynthesis showing how water, light, and carbon dioxide are absorbed by a plant to produce oxygen, sugars, and more carbon dioxide. (Encyclopedia Britannica, 2021 https://www.britannica.com/)

5.1 Original version

There are no algorithms for estimating leaf photosynthesis. In the reference version this algorithm is not needed for calculations, and plants are represented by the following vegetation parameters, which are read in by the model as *external 2D fields* coming from remote sensing data. The vegetation parameters, which are read in, are leaf area indexes, plant coverage, minimum stomatal resistance, root depth and roughness length.

5.2 Updated version

The new leaf photosynthesis algorithm for TERRA-ML is based on the Farquhar and Collatz models for C_3 and C_4 plants (Farquhar et al., 1980; Collatz et al., 1991) and uses sunlit and shaded leaves parameters:

$$A_{can} = A^{sun} L^{sun} + A^{sha} L^{sha} \qquad (20)$$

where: A^{sun} and A^{sha} are values of photosynthesis for sunlit and shaded leaves. According to the CLM strategy (Oleson et al., 2010), the minimum rate set by one of the limiting relations controls CO_2 assimilations at the leaf level:

$$A = min(w_c, w_j, w_e) \qquad (21)$$

where: w_c, w_j, w_e are limiting factors related to the rate of CO_2 fixation in the carboxylation of RuBP in the Calvin cycle, the maximum rate of carboxylation allowed by the capacity to regenerate RuBP, and the capacity for export or utilisation of the carbohydrates, respectively.

$$w_c = \begin{cases} \frac{V_{cmax}(c_i - \Gamma_*)}{c_i + K_c \left(1 + \frac{O_i}{K_0}\right)}, & \text{for } C_3 \text{ plants} \\ V_{cmax}, & \text{for } C_4 \text{ plants} \end{cases} \qquad (22)$$

$$w_j = \begin{cases} \frac{(c_i - \Gamma_*)4.6\alpha PAR}{c_i + 2\Gamma_*}, & \text{for } C_3 \text{ plants} \\ 4.6\phi\alpha, & \text{for } C_4 \text{ plants} \end{cases} \qquad (23)$$

$$w_e = \begin{cases} 0.5 V_{c,max}, & \text{for } C_3 \text{ plants} \\ 4000 V_{c,max} \frac{c_i}{P_{atm}}, & \text{for } C_4 \text{ plants} \end{cases} \qquad (24)$$

where: Γ_* and O_i are CO_2 compensation point and partial pressure, respectively; K_c and K_o are Michaelis-Menten constants for CO_2 and O_2 depending exponentially on T_v; α is quantum efficiency; V_c, max is maximum rate of carboxylation varying among plant functional types and with sunlit and shaded leaves; c_i is internal leaf CO_2 partial pressure; PAR is absorbed photosynthetically active radiation, which is converted to photosynthetic photon flux assuming 4.6 $\mu mol\ photonos\ per\ Joule$.

CO_2 compensation point and O_2 partial pressure:

$$\Gamma_* = \frac{1}{2} \frac{K_c}{K_o} 0.21 O_i, \qquad\qquad O_i = 0.209 P_{atm} \qquad (25)$$

where: the term 0.21 represents the ratio of maximum rates of oxygenation to carboxylation, which is virtually constant with temperature.

$Michaelis\text{-}Menten\ constants\ for\ CO_2\ and\ O_2$:

$$K_c = K_{c25}\alpha_{kc}^{\frac{T_v - 25}{10}}, \qquad\qquad K_o = K_{o25}\alpha_{ko}^{\frac{T_v - 25}{10}} \qquad (26)$$

where: K_{c25} and K_{o25} are values at 25 °C; α_{kc} and α_{ko} are relative changes in K_{c25} and K_{o25}, respectively.

$Maximum\ rate\ of\ carboxylation\ V_{c,max}$: The maximum carboxylation rate ($V_{c,max}$) is a key parameter in determining the plant photosynthesis rate per unit of leaf area. This parameter explains the dependency of photosynthesis rate and couples stomatal resistance algorithm

with environmental parameters. The new algorithm calculates $V_{c,max}$ separately for sunlit and shaded leaves. The maximum rate of carboxylation in algorithm varies with: vegetation temperature, soil water content, function of daylength and the maximum rate of carboxylation at 25 °C:

$$V_{c,max} = V_{c,max_{25}} \alpha_{v_{max}}^{\frac{T_v-25}{10}} f(T_v) f(DYL) f(N) F_{wat} \tag{27}$$

where: $f(T_v)$ is function that mimics a thermal inhibition of RuBisCO activity at temperatures exceeding 35 °C; $f(DYL)$ is function that scales $V_{c,max}$ for daylength and introduces seasonal variation of $V_{c,max}$; F_{wat} is transpiration factor describing the influence of soil water content on $V_{c,max}$ (Eq.11). This function has values in range from one (wet soil) to near zero (dry soil). $f(N)$ scales $V_{c,max}$ for nitrogen limitation; $\alpha_{v_{max}}$ is nitrogen availability factor considers N limitation of $V_{c,max}$ and varies among $PFTs$; $V_{c,max_{25}}$ is maximum rate of carboxylation varies with foliage nitrogen concentration and specific leaf area at 25 °C for sunlit and shaded leaves.

$$f(T_v) = \left[1 + exp \left(\frac{-220000 + 710 \left(T_v + T_f \right)}{0.001 R_{gas} \left(T_v + T_f \right)} \right) \right]^{-1} \tag{28}$$

where: T_v and T_f are vegetation and freezing temperatures.

$$f(DYL) = \frac{DYL^2}{DYL^2_{max}} \tag{29}$$

where: DYL is daylength in seconds. The daylength function has values in range $0.01 \leq f(DYL) \leq 1$.

$$DYL = 2 * 13750.9871 cos^{-1} \left[\frac{-sin(lat) * sin(decl)}{cos(lat) * cos(decl)} \right] \tag{30}$$

where: lat is latitude; $decl$ is declination angle; DYL_{max} is maximum daylenght. It is calculated similarly but using the maximum declination angle for present-day orbital geometry ($\pm 23.4667°[\pm 0.409571$ radians]), positive for Northern Hemisphere latitudes and negative for Southern Hemisphere). The maximum rate of carboxylation varies with foliage nitrogen concentration and specific leaf area at 25 °C is calculated as:

$$V_{c,max_{25}} = N_a F_{LNR} F_{NR} \alpha_{R25} \tag{31}$$

where: N_a is area-based leaf nitrogen concentration; F_{LNR} is fraction of leaf nitrogen in Rubisco; $F_{NR} = 7.16$ is mass ratio of total Rubisco molecular mass to nitrogen in Rubisco; $\alpha_{R25} = 60$ is specific activity of Rubisco.

$$N_a = \frac{1}{CN_L * SLA} \tag{32}$$

where: CN_l is leaf carbon-to-nitrogen ratio and SLA is specific leaf area for sunlit and shaded leaves.

The internal leaf CO_2 partial pressure: The CO_2 partial pressure at the leaf surface c_s and the vapor pressure at the leaf surface e_s, needed for the stomatal resistance model in Eq.14, and internal leaf CO_2 partial pressure c_i, needed for the photosynthesis model in Eqs. 34–36, are calculated assuming there is negligible capacity to store CO_2 and water vapor at the leaf surface. The set of equations is solved separately for sunlit (A^{sun}, r_s^{sun}) and shaded (A^{sha}, r_s^{sha}) leaves, where average absorbed photosynthetically active radiation (PAR^{sun}, PAR^{sha}) and specific leaf area (SLA^{sun}, SLA^{sha}) and hence (V_{cmax}^{sun} and V_{cmax}^{sha}) vary between sunlit

and shaded leaves. Moreover, this equation set is iterated three times (except leaf boundary resistance).

$$A = \frac{c_a - c_i}{(1.37r_b + 1.65r_s)P_{atm}} = \frac{c_a - c_s}{1.37r_b P_{atm}} = \frac{c_s - c_i}{1.65r_s P_{atm}} \tag{33}$$

and the transpiration fluxes are related as:

$$\frac{e_a' - e_i}{(r_b + r_s)} = \frac{e_a' - e_s}{r_b} = \frac{e_s - e_i}{r_s} \tag{34}$$

where: the terms 1.37 and 1.65 are the ratios of diffusivity of CO_2 to H_2O for the leaf boundary layer resistance and stomatal resistance; c_a is atmospheric CO_2 partial pressure; e_i and e_a' are saturation and air vapor pressure.

$$c_a = 355 * 10^{-6} P_{atm} \tag{35}$$

$$c_i = \begin{cases} 0.7c_a, & \text{for } C_3 \text{ plants} \\ 0.4c_a, & \text{for } C_4 \text{ plants} \end{cases} \tag{36}$$

After the first calculations of leaf photosynthesis and stomatal resistance (the first iteration) subsequent values for c_i, c_a are given by:

$$c_i = c_s - 1.65r_s P_{atm} A \tag{37}$$

where: c_s is CO_2 partial pressure at the leaf surface.

$$c_s = c_a - 1.37r_b P_{atm} A \tag{38}$$

where: c_a is atmospheric CO_2 partial pressure calculated from CO_2 concentration.

$$e_a' = \begin{cases} max\left(min\left(e_a, e_i\right), 0.25e_i\right), & \text{for } C_3 \text{ plants} \\ max\left(min\left(e_a, e_i\right), 0.40e_i\right), & \text{for } C_4 \text{ plants} \end{cases} \tag{39}$$

$$e_a = \frac{P_{atm}q_s}{0.622} \tag{40}$$

where: q_s - is the specific humidity of canopy air. Substitution of Eq.33 and Eq.34 into Eq.14 yields stomatal resistance (r_s) as a function of photosynthesis (A) is:

$$\left(\frac{mAP_{atm}e_a'}{c_s e_i} + b\right)r_s^2 + \left(\frac{mAP_{atm}r_b}{c_s} + br_b - 1\right)r_s - r_b = 0 \tag{41}$$

where: r_b is leaf boundary layer resistance,

$$r_b = \frac{1}{C_v} * \left(\frac{U_{av}}{d_{leaf}}\right)^{-\frac{1}{2}} \tag{42}$$

where: C_v is the turbulent transfer coefficient between the canopy surface and canopy air $C_v = 0.01$; d_{leaf} is characteristic dimension of the leaves in the direction of wind flow (constant); U_{av} velocity of air within foliage. It should be noted that all parameters which are required for calculation of boundary layer resistance are in TERRA-ML.

6 Leaf approach

6.1 Original version

A canopy layer is presented as one big leaf. In this approach, all leaves of the canopy have the same plant physiological properties and relative responses to the environment as any single unshaded leaf in the upper canopy. Additionally, in COSMO-CLM, there are several assumptions simplifying this approach. The first one is the moisture flux between the plant foliage and the air inside the canopy to be equal to the flux between the air inside and the air above the canopy. The second one is the foliage temperature to be equal to the surface temperature.
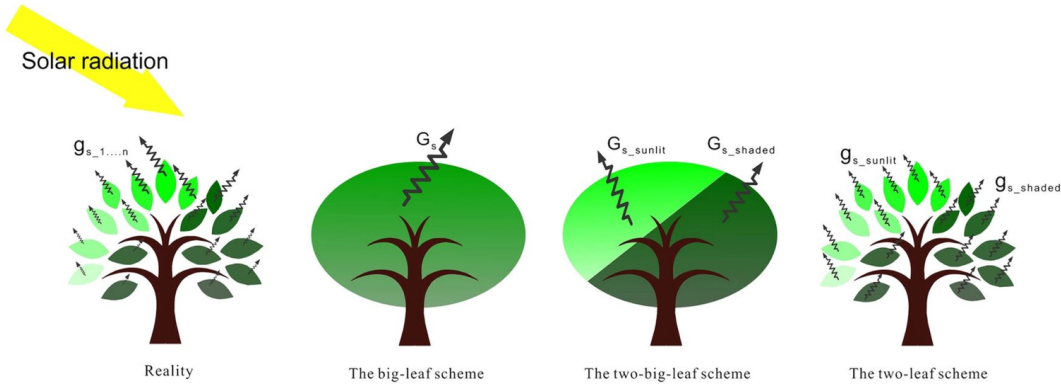

Figure 4: Schematic description of the three upscaling schemes: one-big leaf, two-big leaf and two-leaf scheme according to (Luo et al., 2018)

Impossible integration of the physiological properties between leaves in the overstory, influenced by high irradiance, and leaves in the understory at low light conditions can be considered as a major disadvantage of the one-big-leaf. As such, these result in inaccuracies in the estimation of plant transpiration and leaf photosynthesis (Wang and Leuning, 1998; Dai et al., 2004, Uebel, 2015).

6.2 Updated version

The new description of the canopy layer of COSMO-CLM is presented as a two big leaves approach. Due to the implementation of photosynthesis and stomatal resistance algorithms, we had to substitute the one big leaf approach with the two big leaves one. The main difference between both approaches is that the two-big leaf approach considers different properties of both sunlit and shaded leaves and allows for more accurate calculations of stomatal resistance and leaf photosynthesis rate.
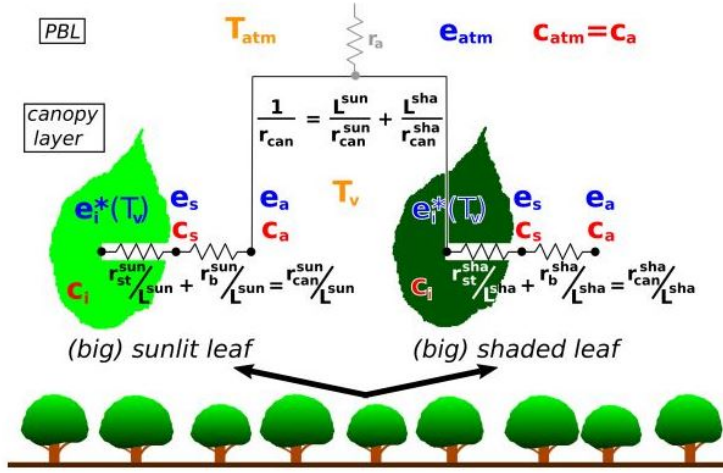
Figure 5: Canopy resistances for photosynthesis and transpiration at the canopy scale described with a two-big-leaf canopy integration scheme according to (Uebel, 2015)

According to this scheme, sunlit leaves receive (absorb) direct beam and diffuse solar radiation. Shaded leaves receive (absorb) only scattered diffuse solar radiation. Applying the two big leaves approach allows for calculating the LAI separately for sunlit and shaded leaves, which is necessary for calculating leaf photosynthesis and stomatal resistance:

$$L_{sun} = f_{sun}L, \qquad\qquad L_{sha} = f_{sha}L \qquad (43)$$

Here, L is leaf area index; and f_{sun} and f_{sha} are sunlit and shaded leaves fractions, respectively, which vary through the daytime and the year. Leaves fractions can be calculated based on solar zenith angle (μ) and the relative projected area of leaves and stems in the direction $cos^{-1}\mu$.

$$f_{sun} = \frac{1 - e^{-KL}}{KL}, \qquad\qquad f_{sha} = 1 - f_{sun} \qquad (44)$$

where: K is the light extinction coefficient; e^{-KL} is the fractional area of sunflecks on a horizontal plane below the leaf area index. Mathematical expression KL should be less then 40.

$$K = \frac{G_\mu}{\mu} \qquad (45)$$

where: G_μ is the relative projected area of leaf and stem elements in the direction $cos\mu^{-1}$.

$$G_\mu = \phi_1 + \phi_2\mu \qquad (46)$$

where: ϕ_1 and ϕ_2 are coefficients; μ is solar zenith angle:

$$\phi_1 = 0.5 - 0.633X_l - 0.33X_l^2, \qquad\qquad \phi_2 = 0.877(1 - 2\phi_1) \qquad (47)$$

where: X_l is the departure of leaf angles from a random distribution and equals:

- **+1** for horizontal leaves
- **0** for random leaves
- **1** for vertical leaves

To prevent numerical instabilities, when $L \leq 0.01$ or the sun is below the horizon $\mu \leq 0$:

$$f_{sun} = 1 \qquad f_{sha} = 0 \qquad L_{sun} = L \qquad L_{sha} = 0$$
$$f_{sun} = 0 \qquad f_{sha} = 1 \qquad L_{sun} = 0 \qquad L_{sha} = L \qquad (48)$$

The implementation of the two big leaves approach requires the development of new algorithms for calculating photosynthetic active radiation (PAR) and specific leaf area (SLA) indexes for sunlit and shaded leaves, which can be used to estimate the reproductive strategy of a particular plant.

$$\phi^{sun} = \frac{\phi_{dir}^{\mu} + \phi_{dif}^{\mu} f_{sun} + \phi_{dif} f_{sun}(\frac{L}{L+S})}{L_{sun}} \qquad (49)$$

$$\phi^{sha} = \frac{\phi_{dif}^{\mu} f_{sha} + \phi_{dif} f_{sha}(\frac{L}{L+S})}{L_{sha}} \qquad (50)$$

Here, ϕ_{dir}^{μ}, ϕ_{dif}^{μ}, ϕ_{dif} are the direct, diffuse downward, and diffuse upward components of photosynthetic active radiation at the ground, respectively.

$$SLA^{sun} = \frac{-(cSLA_m KL + cSLA_m + cSLA_o K - SLA_m - SLA_o K)}{K^2 L^{sun}} \qquad (51)$$

$$SLA^{sha} = \frac{L(SLA_o + \frac{SLA_m L}{2}) - SLA^{sun} L^{sun}}{L^{sha}} \qquad (52)$$

Here, SLA_o is the value for SLA at the top of the canopy; SLA_m is a linear slope coefficient varying among different $PFTs$; c is the recalculation coefficient; and K is the light extinction coefficient. The algorithm for calculation two-big leaf parameteres are presented in module `src_phenology`, subroutine `get_stomatal_data`.

7 Leaf area index

7.1 Original version

There are no algorithms for computation of LAI and vegetation cover fraction ($PLCOV$). These fields are computed and transmitted into TERRA-ML as the minimum and maximum values from the external parameter tool EXTPAR in accordance with the spatial resolution of COSMO-CLM model grid, representing grass at rest and during the growing season. The values of LAI and vegetation ratio follows the same sinusoidal fitted curve between its maximum and minimum value each year, neglecting any influence or feedback on the environmental conditions.

7.2 Updated version

The new algorithm for LAI is based on the LST approach of the SURFEX model (Calvet et al., 2004). The new algorithm allows to calculate changes in LAI depending on biomass evolution due to leaf photosynthesis activity. With a dynamic representation of LAI, the COSMO-CLM model is able to account for interannual variability, droughts in particular. It should be noted that in SURFEX model, the vegetation biomass is expressed in units of *kg of dry matter per m^2* because of the leaf photosynthesis values have to convert at the same units. In the new version of LAI algorithm there is a single biomass reservoir (B), representing the photosynthetic active biomass, including the leavess and also a proportion

of the stem and roots, which provide water for transpiration. Once a day, at midnight, both growth and mortality is calculated:

$$B(t + \Delta t) = B(t) + \Delta B^+ - \Delta B^- \tag{53}$$

The growth is based on the accumulated net CO_2 assimilation over the previous day:

$$\Delta B^+ = \frac{M_c}{P_c M_{CO_2}} A_{nI,day} \Delta t \tag{54}$$

where, M_C and M_{CO_2} are the molecular weights of carbon and CO_2; P_c is the proportion of carbon in the dry plant biomass equal to 0.4; $A_{nI,day}$ is the daily accumulated A_{nI}. Also, the new algorithm considers mortality due to soil moisture stress, diseases and senescene. It is given by an exponential extinction of B characterized by a time-dependent effective life expectancy:

$$\Delta B^- = B \left(1 - exp \left[\frac{\Delta t}{\tau} \right] \right) \tag{55}$$

and

$$\tau(t) = \tau_M \frac{A_{nfm}(t)}{A_{n,max}} \tag{56}$$

where τ_M is the maximum effective life expectance, depending on vegetation type; A_{nfm} is the maximum leaf A_n reached on the previous day and $A_{n,max}$ is the optimum leaf A_n. The LAI is obtained from biomass assuming a constant ratio, depending on vegetation type:

$$LAI = \frac{B}{\alpha_B} \tag{57}$$

8 Results

In order to analyse the changes in COSMO-CLM related to the changes in stomatal resistance and leaf photosynthesis algorithms described above, we carried out experiments with the COSMO-CLM v5.16. We analysed climatological annual and daily cycles of the model variables from 2010 to 2015 for three small study domains (*Parc* with coordinates 50.8N-50.9N $\times$ 6.38E-6.60E, *Linden* 50.2N-50.8N $\times$ 8.4E-8.8E, and *Lindenberg* 52.2N-52.4N $\times$ 14.0E-14.4E) with mixed grass biome types. Mixed means that grass was combined with crops or surrounded by them. The results of the experiments are based on the one-dimensional model version presented in the vertical soil-vegetation-atmosphere column. This set-up allows for the study of surface and vegetation exchange processes and avoids large-scale atmospheric effects. The one-dimensional version allows for more accurate interpretation of the results on vegetation-atmosphere interactions, as horizontal advection can be ignored. The focus of the analysis was on evaluation of the COSMO-CLM output parameters (e.g., stomatal resistance ($RSTOM$); total evapotranspiration ($ZVERBO$); amount of water evaporation ($AEVAP$); latent and sensible heat fluxes ($ALHFL$, $ASHFL$); and air temperatures: near surface, minimum and maximum T_{2m}, T_{min}, and T_{max}) during the period when the vegetation is in its active phase since there were no meaningful changes in COSMO-CLM parameters (besides r_s) from September (October) to March (April). The simulation results are presented in the documentation at the Parc domain. The simulation results for Linden and Lindenberg domains had similar outcomes and are moved to the Supplementary materials.

The first simulation (CCLMv3.5) is based on the adapted algorithm of CLMv3.5 for stomatal resistance, which depends on leaf photosynthesis, CO_2 partial and vapor pressure, and maximum stomatal resistance. The second one (CCLMv4.5) is based on the vegetation algorithm

adapted from the CLMv4.5, including the soil water stress function also governing stomatal resistance at night. The last one (CCLMv4.5e) is similar to the experiment (CCLMv4.5) algorithm for stomatal resistance, including additional changes in calculations of transpiration from dry leaf surface. The COSMO-CLM experiments in a one-column mode were tested (for C_3 grass), analysed, and compared:

- to the reference simulation (CCLMref) with the original algorithm;

- with observational sites (when observational data were available) and stomatal resistance values out of the literature;

- with available datasets (TRY, HYRAS and GLEAM).

8.1 Observational data

The observational sites were selected in such a way that they cover similar types of plants (C_3 grass) in different parts of Germany (Fig. 6). Three EURONET sites were selected: two cropland sites (Selhausen Juelich and Selhausen) and one grassland site (Rollesbroich). The EURONET sites are located in the western part of Germany near the Belgian border and are part of the TERENO project. The sites are surrounded either by crops or grass, and according to the TERENO project report (Bogena et al., 2018), the predominant vegetation species are *perennial ryegrass* (*Lolium perenne L.*) and smooth meadow grass (*Poa pratensis L.*). We also used grassland data from the Environmental Monitoring and Climate Impact Research Station Linden, which is located near Giessen, as well as data from the station of Lindenberg Meteorological Observatory of German Meteorological Series. The predominant vegetation species at the Linden site were 12 grass species and can be characterised as an *Arrhenatherum elatius* and *Filipendula ulmaris* sub-community, and at Lindenberg were perennial ryegrass (*Lolium perenne*) and red fescrue (*Festuca rubra*). A detailed description of instrumentation, the measurement conditions, and quality control procedures is given for EURONET sites by Bogena et. al. (2018), for Linden site by Bruns et al. (2003), and for Lindenberg by Beyrich and Adam (2007). Forest sites were not taken into account at this stage of the research, as algorithms for grass only were implemented into the COSMO-CLM model.

As an additional source of data for evaluating model results, we used the observational gridded datasets (HYRAS, Frick et al., 2014 and GLEAM, Martens et al., 2017) with information about precipitation, temperature, and evaporation for validation of COSMO-CLM parameters and global TRY database (Kattge et al., 2020) with different characteristics of plants (stomatal conductance, leaf photosynthesis, and maximum rate of carboxylation data). That allowed us to obtain more precise statistical scores because the models and gridded observational datasets represent average values rather than processes in specific points (Osborn and Hulme, 1998).
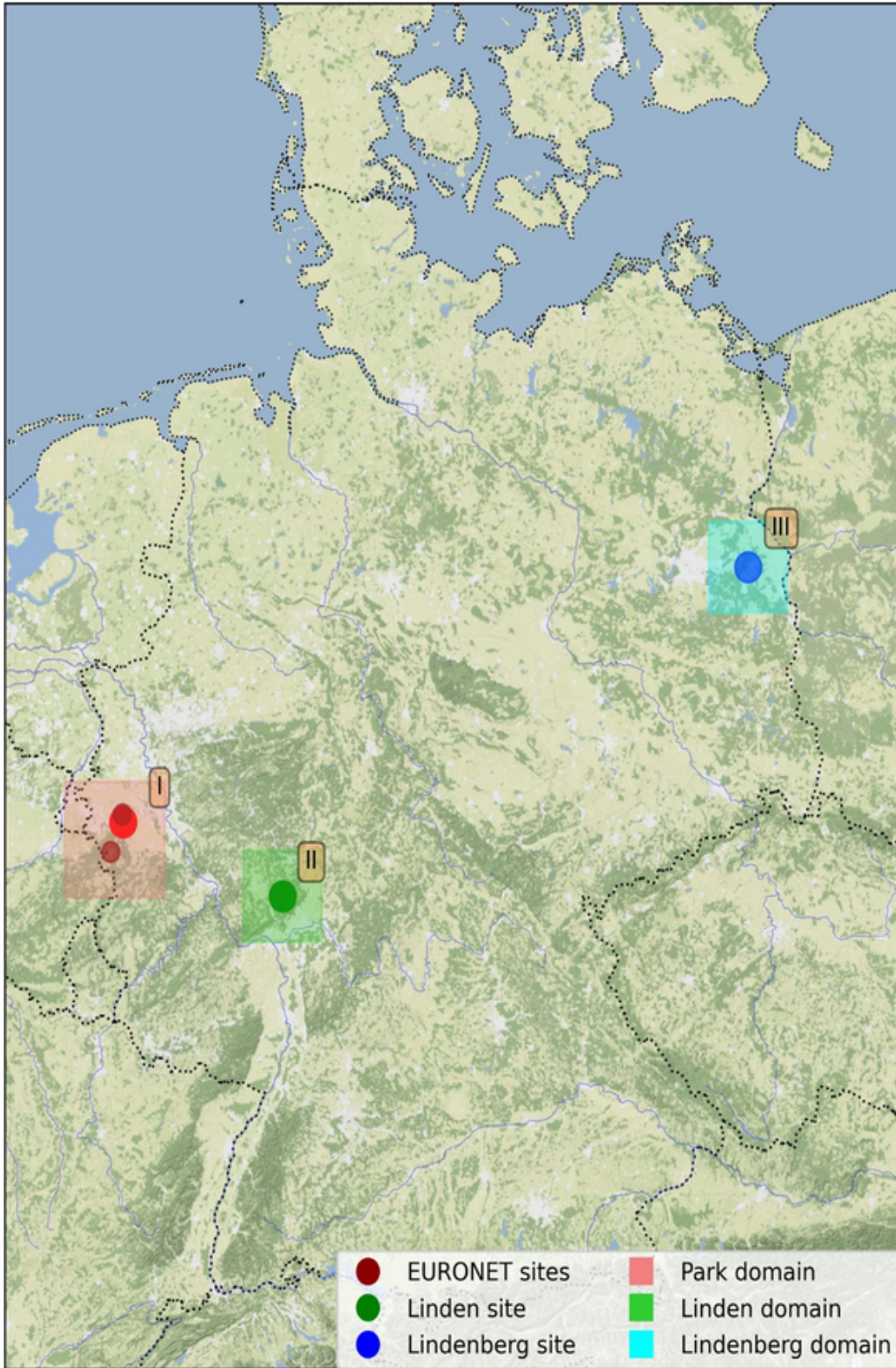
Figure 6: The sites and research domains over Germany. An initial layer with information about altitudes for the map was obtained from the official webpage of NOAA (https://www.ngdc.noaa.gov/mgg/global/).

8.2 Stomatal resistance

The current algorithm of stomatal resistance based on the Jarvis approach with BATS model parameterisation and the new schemes based on the physical Ball-Berry approach coupled with processes of leaf photosynthesis calculated separately for sunlit and shaded leaves. The results seen in (Fig.7) demonstrate the changes in stomatal resistance (a - daytime, b - night-time) from the grassland surface at Parc domain as boxplots from May to September, as simulated by the reference and the new algorithms in COSMO-CLM. Stomatal resistance from grassland was substantially reduced at daytime by the physical Ball-Berry approach compared to the Jarvis approach (Fig. 7a). However, night-time values of stomatal resistance (Fig. 7b) of the CCLMv3.5 algorithm were considerably overestimated in comparison with the other experiments. This happened because the CCLMv3.5 uses the empirical constant parameter (Sellers et al., 1996) for obtaining $r_{s,max}$, which was set to 20000 s/m for this experiment (Oleson et al., 2010). CCLMv3.5 reached the daily maximum values at night-time when leaf photosynthesis was equal to zero ($A_{night} = 0$), which is consistent with Balls theory (Ball, 1988). The largest differences between the reference simulation (CCLMref) and the experimental simulations (CCLMv3.5, CCLMv4.5, and CCLMv4.5e) were observed from September (October) to March (April), when stomata were closed or there were no leaves. These cases are presented in Supplementary materials (Fig .13). Nevertheless, the changes in stomatal resistance in this period did not have a considerable influence on other COSMO-CLM variables (surface temperature, latent and sensible heat fluxes). This was a logical result as the LAI and therefore the transpiration from grassland was small in the model during this period; because of that, the focus of the research was concentrated on the period from April (May) to September, when vegetation was in the active phase.
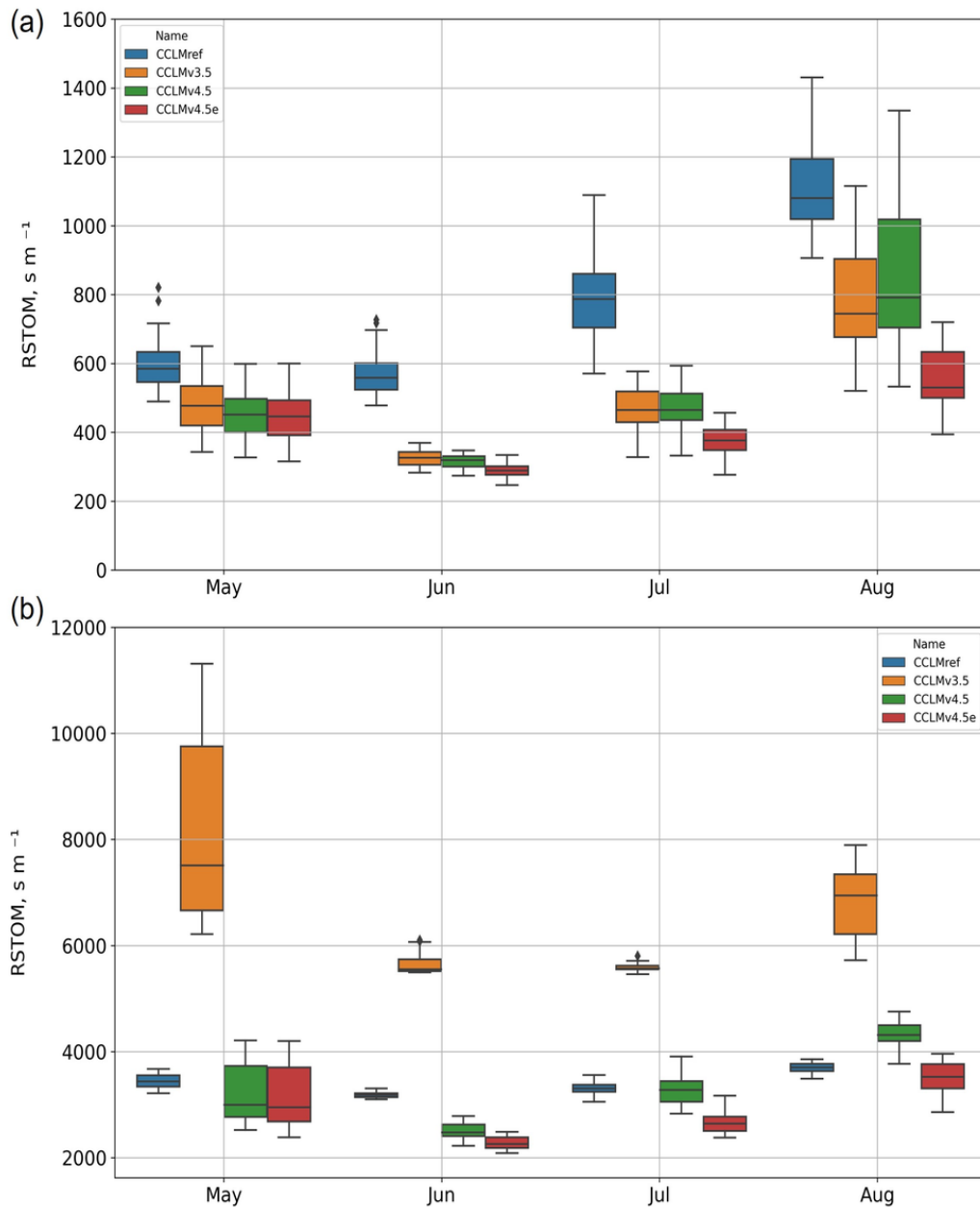
Figure 7: Monthly mean stomatal resistance values ((**a**) daytime, (**b**) night-time) at the Parc domain averaged over the period of 2010-2015: CCLMref (blue box), CCLMv3.5 (orange box), CCLMv4.5 (green box), and CCLMv4.5e (red box).

Stomatal resistance validation of the reference and experimental results presented in time-series format is a formidable task. Due to measuring stomatal resistance (conductance) being a resource-intensive task, especially for its continuous quantification over time and there being no long-term in-situ time series or datasets including daily stomatal resistance data. We analysed different resources and found some published data on in-situ-measured stomatal resistance presented into the *TRY database*. In the TRY database, we found five additional datasets with information from Europe about C_3 grass species (*Lolium perenne*, *Arrhenatherum elatius*, *Festuca rubra*, *Poa pratensis*, and *Festuca rubra*):

- DIRECT Plant Trait (Everwand et al., 2014);

- GLOPNET-Global Plant Trait Network (Wright et al., 2004);

- Global Respiration (Reich et al., 2008);

- Photosynthesis Traits Worldwide (Maire et al., 2016);

- Traits of 59 grassland species (Schroeder-Georgi et al., 2016)

Nevertheless, not all data presented in selected datasets have information about time. Because of that we calculated the correlation coefficients (Fig. 8a) based on COSMO-CLM parameters and found the most important parameters which can be related to stomatal resistance are soil moisture, surface air temperature and total precipitation (such COSMO-CLM parameters as AEVAP, ALHFL and ASHFL are also have important correlation coefficients but they are partly depended on stomatal resistance values). Then we analysed data from the TRY database and found that only several dasets have information about soil moisture and total precipitation, but all datasets have information about temperature. Due to we decided to create four categories of stomatal resistance data depending near surface air temperature. Such as, there is significant correlation coefficient ($r = 0.62$) between r_s and T_{air}. The results (Fig. 8b) show that the experiments based on the algorithms, which take into account the role of leaf photosynthesis, CO_2 concentration, and environmental parameters (e.g., air near-surface temperature and humidity, soil water, active radiation), have r_s values smaller than the CCLMref. The CCLMv4.5e experiment with the additional changes in the algorithm for calculations of transpiration from dry leaves demonstrated better accuracy than the other experiments.
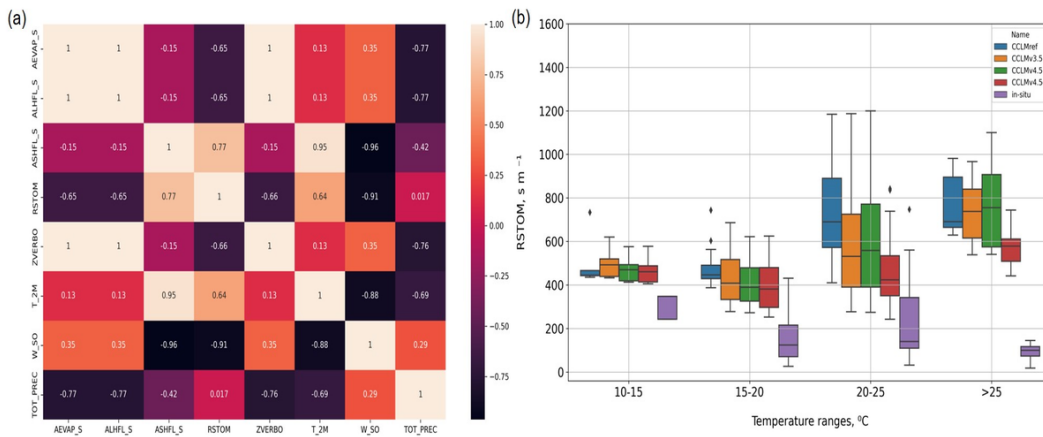

Figure 8: Daily daytime mean values of stomatal resistance values at the Parc domain averaged over the period 2010–2015 presented on the COSMO-CLM parameters correlation heatmap (**a**) and divided into 4 categories depending on near-surface air temperatures (**b**): CCLMref (blue box), CCLMv3.5 (orange box), CCLMv4.5 (green box), CCLMv4.5e (red box), and in-situ data (purple box).

From Figures 7-8, it becomes clear that the daytime stomatal resistance values of the new algorithms were smaller than the reference and more accurately described stomatal resistance in comparison with in-situ measurements. The smallest value of stomatal resistance was found in CCLMv4.5e. The experiment CCLMv3.5 overestimated values of stomatal resistance at night. The changes in stomatal resistance algorithm should be visible on the other output parameters of COSMO-CLM. In particular, the total evapotranspiration and the amount of water evaporation should increase.

8.3 Evapotranspiration and evaporation

According to Davin and Seneviratne (2012), there is a tight coupling between photosynthesis and transpiration. It is a fact that transpiration is the main contributor to land evapotranspiration (Matheny et al., 2014). Stomatal resistance is also expected to affect water fluxes (Uebel, 2015). We analysed the data from COSMO-CLM, which are related to the total evapotranspiration and the amount of water evaporation, to examine the sensitivity of these parameters to stomatal resistance changes. For validation of model results, we applied the gridded observational datasets GLEAMv3.5a and GLEAMv3.5b. The output results of COSMO-CLM parameters ($AEVAP$ and $ZVERBO$) were estimated near the meteorological stations. The results at the Parc domain are shown in (Fig. 9a and 9b). The comparison of the experiments with GLEAM datasets demonstrated that canopy processes are more realistically represented in the new algorithms (except CCLMv4.5e - $AEVAP$). It can clearly be seen (Fig. 9c) that the performance of CCLMv4.5e was the most accurate for $ZVERBO$ parameter; however, accuracy of $AEVAP$ in this experiment was reduced. The performances of CCLMv3.5 and CCLMv4.5 were typically close to the gridded observation datasets for both parameters, in contrast to CCLMref in our research domains. Motivated by this, we then investigated the performance of the experiments on the basis of gridded data over other domains (including Parc).
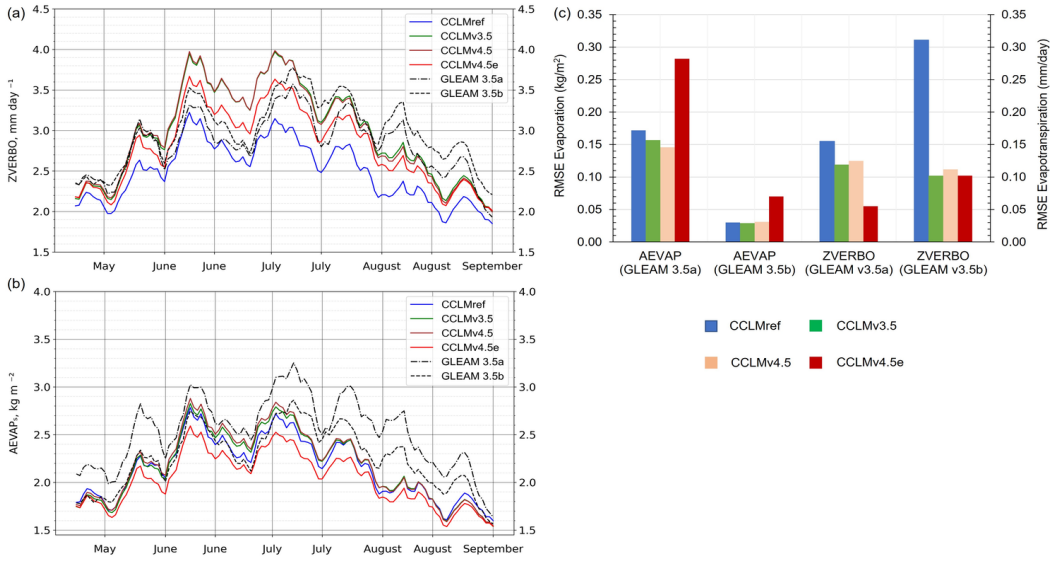

Figure 9: Daily mean total evapotranspiration (**a**), the amount of water evaporation (**b**), and model performance (**c**) at the Parc domain averaged over the period 2010-2015: CCLMref (blue), CCLMv3.5 (green), CCLMv4.5 (brown), CCLMv4.5e (red), GLEAM˙v3.5a (dotted line), and GLEAM˙v3.5b (dashed line). The considered score is the RMSE calculated from the differences (experiment minus observation).

We analysed the experiments and the gridded observational datasets presenting on the COSMO-CLM model grid. For this analysis, we calculated the correlation coefficient; the distribution added value index (DAV) to estimate the Perkins skill scores (S) between reference (subscript ref), experimental (subscript exp), and observational (subscript obs) data; the Kling-Gupta efficiency index (KGE, Fig. 10b) to demonstrate the model (subscript m) effectiveness with respect to the observational time series; and the root mean square deviation ($RMSD$; Fig. 10a).
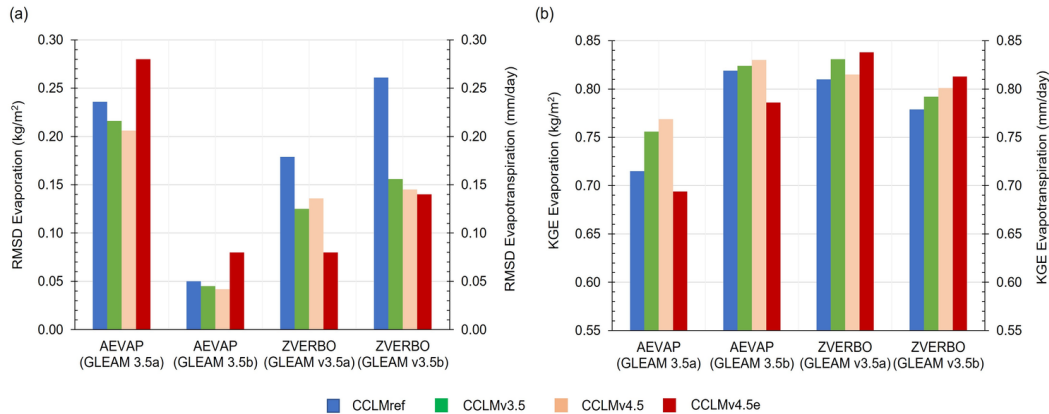
Figure 10: Model performance for daily mean total evapotranspiration and the amount of water evaporation at the Parc domain averaged over the period 2010-2015 for the different model experiments: CCLMref (blue), CCLMv3.5 (green), CCLMv4.5 (brown), and CCLMv4.5e (red). The considered scores are (**a**) the RMSD and (**b**) the KGE taken at each grid cell for each day.

The *KGE* values less than -0.41 demonstrate that there is a lack of precision in relation to the mean of the control (observational) data. *KGE = 1* indicates that there is a perfect matching between experimental and control data (Toelle and Churiulin, 2021). In our experiments, the *KGE* values for *AEVAP* and *ZVERBO* were higher than 0.68 for all the simulations. The highest performance values for GLEAM datasets were obtained for *AEVAP* with the simulation based on the experiment CCLMv4.5 ($KGE_{mean} = 0.80$), and for *ZVERBO* with CCLMv4.5e ($KGE_{mean} = 0.82$). The RMSD for the data presented at the COSMO-CLM grid also confirmed that the CCLMv4.5 experiment had the lowest errors for *AEVAP* ($RMSD_{mean} = 0.124$) and the CCLMv4.5e for *ZVERBO* ($RMSD_{mean} = 0.110$). The spatial correlation coefficients of the simulations with the GLEAM datasets for *AEVAP* and *ZVERBO* were similar and equal to 0.881 for the experiments, and 0.875 for the CCLMref. The simulation results based on the new formulations for *ZVERBO* performed better, and this was proven by the positive *DAV* values (*DAV > 0* show that there was a benefit in using the alternative experiment version compared to the reference with respect to the observations). Experiments CCLMv3.5 (*DAV = 0.023*) and CCLMv4.5 (*0.028*) had positive values of *DAV*, while the CCLMv4.5e had negative values (*-0.022*), indicating that there was either no gain or that we had a loss in performance for the alternative version (Raffa et al., 2021).

8.4 Sensible, latent heat fluxes and air temperatures

We investigated differences between the experiments CCLMref, CCLMv3.5, CCLMv4.5, and CCLMv4.5e for sensible (Fig.11a) and latent heat (Fig. 11b) fluxes and air near-surface (Fig. 12a), minimum (Fig. 12b), and maximum (Fig. 12c) temperatures as daily mean values averaged over the period 2010–2015 at the Parc domain. The comparison of sensible and latent heat fluxes presented on the COSMO-CLM grid (2.2 km distance between grid nodes) with the in-situ data demonstrated that the model experiments differed significantly from the observations. However, we expected these results, since a similar situation was described in the work of Osborn and Hulme (1998). The main positive feedback from these figures (Fig.11a,b) was the fact that there was a connection of sensible and latent heat fluxes with a change in stomatal resistance. For example, if plant stomata were open, it

means that values of stomatal resistance and sensible heat flux decreased, but values of plant transpiration, amount of water evaporation, and latent heat flux increased.

Before validation of the output temperature parameters, we assumed that the changes in them should be minor. The validation and statistical results (STD, MAE, $RMSE$, r) of the output parameters confirmed our assumption. The changes of $RMSE$ are presented in Fig.12d. The Pearson correlation coefficient for all simulations was above 0.98 for surface, 0.93 for maximum temperatures, and 0.92 for minimum temperatures. We also compared the experiments and the gridded observational dataset HYRAS presenting on the COSMO-CLM model grid and calculated statistical indexes KGE, DAV, and $RMSD$. However, the result of such statistical analysis demonstrated that the differences between the temperature simulations were small. The performance values based on KGE for T_S, T_{max}, and T_{min} for all experiments, including the reference experiment, were equal to 0.91, 0.90, and 0.68, respectively. The spatial correlation coefficients of the simulations with the HYRAS observational dataset were similar and equal to 0.99. The DAV values for the experiments were equal to zero, indicating that there were no differences between the experiments and the reference simulation.
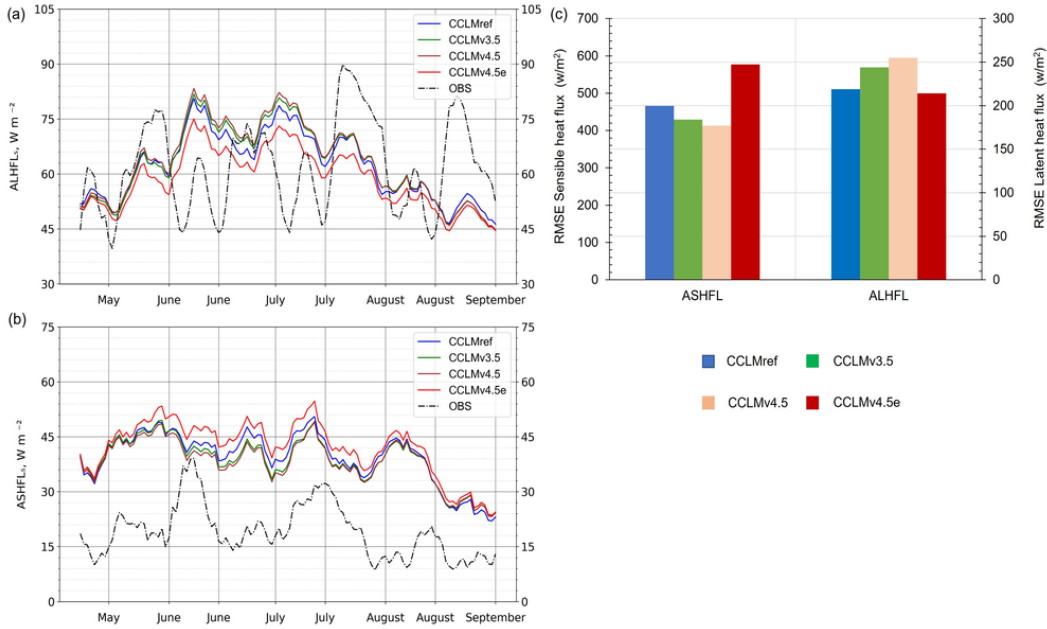

Figure 11: Daily mean latent (**a**) and sensible (**b**) heat fluxes and model performance (**c**) at the Parc domain averaged over the period 2010-2015: CCLMref (blue), CCLMv3.5 (green), CCLMv4.5 (brown), CCLMv4.5e (red), GLEAM˙v3.5a (dotted line) and GLEAM˙v3.5b (dashed line). The considered score is the RMSE calculated from the differences (experiment minus observation).

Figure 12: Daily mean near-surface (**a**), minimum (**b**), maximum (**c**) air temperaturs and model performance (**d**) at the Parc domain averaged over the period 2010-2015: CCLMref (blue), CCLMv3.5 (green), CCLMv4.5 (brown), CCLMv4.5e (red), GLEAM˙v3.5a (dotted line) and GLEAM˙v3.5b (dashed line). The considered score is the RMSE calculated from the differences (experiment minus observation).
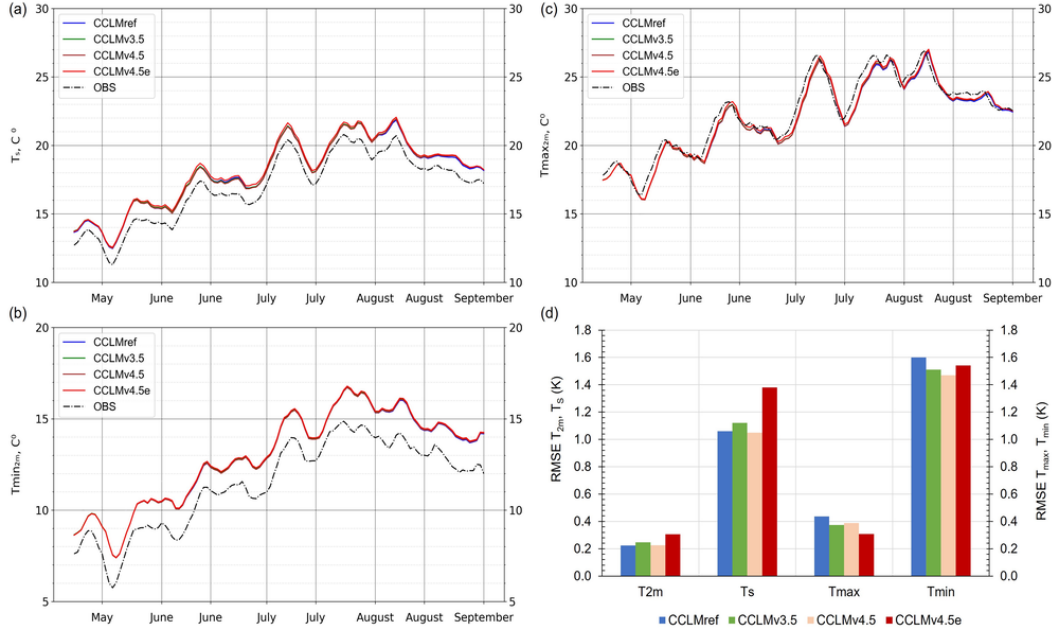
9   Discussion and conclusions

Evapotranspiration is an important component in the energy balance equation, playing a major role in the water cycle that links atmospheric and land surface processes (Dokuchaev, 1899; Schaer et al. 2004). Schulz et al., (2015) and Shrestha and Simmers, (2019) showed that the evapotranspiration simulated by the soil model TERRA-ML of COSMO-CLM was systematically underestimated during the growing season over Europe. A possible cause for underestimated evapotranspiration is that TERRA-ML uses the simplified vegetation parameterisation scheme in which:

- plant canopy has the same temperature as the ground (Doms et al., 2018);

- the incoming solar radiation is directly used to heat the ground (Schulz and Vogel, 2020);

- stomatal resistance algorithm does not consider the role of stomatal regulation and vegetation growth depending on atmospheric CO_2 concentrations and leaf photosynthesis that are especially relevant in global and regional climate changes.

Because of that, we decided to implement into the COSMO-CLM v5.16 (v6.0) the algorithm that allows calculating the stomatal resistance to be more accurate. The new stomatal resistance algorithm implemented in COSMO-CLM is based on the physical Ball-Berry approach coupled with leaf photosynthesis models and is calculated separately for sunlit and shaded leaves. The new one takes into account the difference between physiological properties of sunlit and shaded leaves, as well as physical, biophysical, and biogeochemical processes. The new algorithms allow stomatal resistance to be related to net leaf photosynthesis, scaled

28

by relative humidity and CO_2 concentration. The experiment results were estimated and compared with the reference simulation without changes (CCLMref) and in-situ data. The main results of our study are summarised as follows:

- We compared output COSMO-CLM parameters (transpiration from dry leaf surface, evapotranspiration, latent and sensible heat fluxes, near-surface air temperatures) with gridded datasets, in-situ data, and the reference experiment (CCLMref) without changes over three sites mainly dominated by grass with one-column regional climate model simulations. The validation results of the experiments (CCLMv3.5, CCLMv4.5, CCLMv4.5e) with different stomatal resistance algorithms implemented in COSMO-CLM v5.16 showed that changes in the vegetation algorithm increased the accuracy of other parameters of the COSMO-CLM model by comparing them with independent data. The statistical results proved that changes in the vegetation algorithm can improve the accuracy of other output parameters of COSMO-CLM v5.16 (v6.0). In our research, the experiment CCLMv4.5 showed slightly better statistical results than other experiments (CCLMv3.5, CCLMv4.5) and the reference (CCLMref). This experiment is much more sensitive to changes in environmental conditions (e.g., soil moisture deficit, warm temperatures, CO_2 concentrations) and uses the minimal numbers of constant values. Because of that we decided to implement this algorithm into the new version of COSMO-CLM v6.0.

- Experiments with COSMO-CLM model show that there are opportunities for further modernisation of the regional climate model COSMO-CLM (e.g. implementation of the new PFT, implementation more dynamic parameters with are related to boundary layer resistance into TERRA-ML, modernisation of the algorithm for calculation water vapor flux between the plant foliage, and the canopy air, implementation the new algorithm for calculating the foliage temperature). All these updates can help to additionally improve the accuracy of COSMO-CLM computations, however all of them are requiring more extensive updates and technical developments, which are not the subject of this study and need careful evaluation in a step-by-step manner.

- Based on the experiments results from the COSMO-CLM v5.16 we defined the best algorithm for computation changes in vegetation. Due to only one version - CCLMv4.5 was fully implemented into COSMO-CLM v6.0 and published into COSMO gitlab repository as a new branch. The new version cannot be calculated on GPU proccesors and there are no algorithm for parallelisation, because there are a lot problems with model evaluation in this mode.

- More detailed information about the estimation of experiment results are presented in *Section Presentations*.

10 Changes in COSMO-CLM v6.0 model code (technical aspects)

10.1 Calculation of the new vegetation parameterization scheme:

The new vegetation scheme is based on the vegetation algorithm adapted to COSMO-CLM v6.0 from the CLMv4.5. The detailed description of the implemented algorithms can be found in Sections 2 and 3 of the current documentation. The new algorithms are presented in the `src_phenology.f90` module and divided on the six different subroutines. All subroutines calls from TERRA-ML.

- `src_phenology.f90`.

  The new module has six different subroutines for calculating vegetation parameters:

  1. `get_stomatal_grid` - subroutine for calculating special (virtual) grid with information about actual plant types. The new vegetation scheme has been tested only for C_3 grass. In case of further modernization, the new algorithm for definition of actual PFT should be implemented here;

  2. `get_sun_data` - subroutine for calculating additional physical parameters, required for stomatal resistance calculations. The focus in this subroutine made on calculations of additional solar characteristics;

  3. `get_stomatal_data` - subroutine for calculating additional physical parameters unavailable in COSMO-CLMv6.0 model for stomatal resistance calculations. This subroutine has the two big leaf approach and calculates output parameters both for sunlit and shaded leaves;

  4. `stomata` - subroutine for calculating stomatal resistance based on the physical Ball-Berry approach coupled with leaf photosynthesis models. Subroutine should be called from TERRA-ML separately for sunlit and shaded leaves;

  5. `respiration` - subroutine for calculating such parameters as total plant respiration, gross and net primary production;

  6. `biomass_evolution` - subroutine for calculating of leaf area index (LAI) depending on biomass evolution. Algorithm based on the SURFEX model parameterization scheme and require accumulation of output parameters.

The new `src_phenology` module uses constant and special PFT parameters. These values are presented in the next new module.

- `src_phenology_data.f90`.

  This module declares and initializes all constant and PFT parameters required for the `src_phenology.f90`. At the moment, module has PFT parameters for C_3 and C_4 grass presented in two tables `pft_CN_par` (parameters for PFT from CLM model) and `pft_SURFEX` (parameters for PFT from SURFEX model). The new PFT parameters should be added to both table in the case of modernization or extension of available PTF types. Also, module has two subroutines `phenology_wkarr_alloc` and `phenology_wkarr_dealloc` for allocation and deallocation local parameters in case if `ALLOC_WKARR` mode is active.

- `sfc_terra_data.f90`.

  The new module `src_phenology` is called in TERRA-ML because of that several additional changes implemented in it:

  1. Added the logical parameter *lphenology* in TERRA-ML for optional activation of the new vegetation parameterization scheme;

  2. Added option for calculating stomatal resistance based on standard (Jarvis) or more modern physical based Ball-Berry approach;

  3. Changed the visibility status of TERRA-ML parameters such as: *ZTRALEAV* and *ZVERBO* from local TERRA-ML parameter to global;

  4. Added 20 new local TERRA-ML parameters which have to be used in `src_phenology.f90`;

5. Added 25 new global parameters. 7 of them have type - intent **IN**, 4 - intent **INOUT** and 15 - intent **OUT**;

6. Added new call for the new subroutines from *src_phenology.f90* module.

10.2   New diagnostics fields:

The new diagnostics fields have been implemented by Evgenii Churiulin for the new vegetation parameterization scheme. The following list gives the I/O shortnames, the new variable names and also the former names used in the new vegetation parameterization scheme. All new output fields were implemented and tested only in NetCDF format. The output format GRIB2 is not available for the new fields. Information about new fields have been added in the variable table *src_setup_vartab.f90*:

Shortname	Element Number	Table type	Level type	Time Range Indicator	Variable name
ZTRALEAV	202	202	1	0	ztraleav
ZVERBO	236	202	1	0	zverbo
AZTRALEAV	237	202	1	3	aztraleav
AZVERBO	238	202	1	3	azverbo
SFLDIR_PAR	239	202	1	0	sfldir_par
SFLDIFD_PAR	240	2	1	0	sfldifd_par
SFLDIFU_PAR	240	201	1	0	sfldifu_par
COSZ	241	2	1	0	cos_zen_ang
ASFLDIR_PAR	242	202	1	3	asfldir_par
ASFLDIFD_PAR	243	2	1	3	asfldifd_par
ASFLDIFU_PAR	243	201	1	3	asfldifu_par
SUR_LAI	243	202	1	4	sur_lai
SUR_PANFM	244	2	1	4	sur_panfm
SUR_PANDAY	249	2	1	4	sur_panday
SUR_BIOMASS	244	201	1	4	sur_biomass
SLA_SUN	244	202	1	0	sla_sun
SLA_SHA	245	2	1	0	sla_sha
LAI_SUN	245	201	1	0	lai_sun
LAI_SHA	245	202	1	0	lai_sha
VC_SUN	246	2	1	0	vcmax_sun
VC_SHA	246	201	1	0	vcmax_sha
PAR_SUN	246	202	1	0	par_sun
PAR_SHA	247	2	1	0	par_sha
RS_LEAF	247	201	1	0	rs_leaf
LEAF_PSN	247	202	1	0	psn
GPP	248	2	1	0	gpp_flux
NPP	248	201	1	0	npp_flux

Table 1: New output parameters in *src_setup_vartab.f90*

10.3   Changes to the Namelists:

It was important to create opportunity for choosing between the reference stomatal resistance algorithm based on the Jarvis approach and the new vegetation parameterization scheme based on the Ball-Berry approach coupled with leaf photosynthesis and two big leaves approach. Therefore, we have implemented a logical parameter *lphenology*. The parameter was declared into *data_runcontrol.f90* and set as an additional parameter of the **PHYCTL** namelist into *organize_physics.f90*. Also, in the *organize_physics.f90* there is additional error notification that the new vegetation scheme doesnt work on GPU processors.

Group	Name		Meaning	Default
/PHYCTL/	lphenology	NEW	if .TRUE., the new vegetation parameterization scheme is activated.	.FALSE.

Table 2: New namelist parameters in **PHYCTL**

10.4   Additional technical changes and bug fixes:

Implementation of the new vegetation parameterization scheme for vegetation is required a lot of technical changes:

- *data_fields.f90*.

  The fields for calculation of the new vegetation and radiation parameters were added to the *data_fields* module. All new data fields are located in the 14th section.

- *sfc_allocation.f90*.

  Added the new section for parameters from the 14th section of *data_fields.f90*. All data fields for calculations of the new vegetation and radiation parameters are allocated in subroutine *alloc_meteofields* and deallocated in subroutine *dealloc_meteofields*.

- *data_block_fields.f90*.

  Most of the new parameters have to be used in *sfc_terra.f90* module with a special data block structure due to we declared them into *data_block_fields.f90* module. All new data fields with the block structure are located in the 11th section.

- *src_block_fields_org.f90*.

  Added the new data fields used in *sfc_terra.f90* to current module from *data_fields.f90* and *data_block_field.f90*. The data fields with *_b* structure are allocated in *block_fields_allocate* and deallocated in *block_fields_deallocate* subroutines. Also, new parameters have been added to the *block_fields_register_all* subrotune for registering them with block fields with corresponding *i,j,k* fields.

- *sfc_interface.f90*.

  1. Added logical parameters lphenology and vegetation parameters with *_b* and *_t* structures;
  2. Allocated and deallocated new parameters with *_t* structure in subroutines *sfc_in_wkarr_alloc* and *sfc_in_wkarr_dealloc*;

3. Added new field to subroutine `sfc_init_copy`;

4. Added new parameters for subroutines terra and `tile_averaged_ground`. Most of the new parameters have special type *OPTIONAL*;

5. Added new data fields to section *copy the land points back to the blocked format*.

- `sfc_tilechar_approach.f90`.

  Added tile-dimension to 18 variables for the new vegetation scheme.

- `radiation_interface.f90`.

  Added logical parameter lphenology and new parameters for calculating direct (`sfldir_par`), diffuse downward (`sfldifd_par`), diffuse upward (`sfldifu_par`) components of photosynthetic active radiation and cosine of solar zenith angle (`cos_zen_ang`) based on **fesft** subroutine.

- `organize_data.f90`.

  Added 7 data fields as restart fields in Section 3.3: Initialize the lists for restart variables and defined the rank of the new parameters. Also, accumulated, and averaged fields added to correspondently sections.

- `src_input.f90`.

  Added information about 4 new data fields in Section 2: Put the record into the array *procarray* for definition of **idim3** actual number.

- `src_gridpoints.f90`.

  Added additional parameters for radiation: `sfldir_par`, `sfldifd_par`, `sfldifu_par`.

- `dfi_initialization.f90`.

  1. Added logical parameter *lphenology* for the new vegetation parameterization scheme;

  2. Added vegetation fields (*aztraleav*, *azverbo*).

- `near_surface.f90`.

  1. Added new accumulated variables for solar radiation (`asfldir_par`, `asfldifd_par`, `asfldifu_par`);

  2. Added new accumulated variable for vegetation *aztraleav*, *azverbo*.

10.5 Changes of Results:

The results of TERRA-ML output parameters (e.q., RSTOM, ZTRALEAV, ZVERBO, AE-VAP, ASHFL, ALHFL) might change if the new vegetation parameterization scheme is activated.

11 Supplementary materials

11.1 PFT parameters:

The new vegetation alogrithms use PFT's constant parameters for different plant species. At the moment, the PFT parameters for $C3$ and $C4$ grass have been implemented in COSMO-CLMv6.0 in the module `src_phenology_data.f90`. In case of extension the numbers of PFTs, the new one should be added in this table.

	Parameter	Model name	PFT plant types	
			C3 grass	C4 grass
1	Ratio of momentum roughness length to canopy top height	R_ZOM	0.12	0.12
2	Ratio of displacement height to canopy top height	R_DISP	0.68	0.68
3	Characteristic dimension of the leaves in direction of wind flow	D_LEAF	0.040	0.040
4	Photosynthetic pathway: (C3 = 1.0, C4 = 0.0)	C3_PSN	1.0	0.0
5	Maximum rate of carboxylation at 25C	V_CMX25	52.0	52.0
6	Slope of conductance to photosynthesis relationship	MP	9.0	5.0
7	Quantum efficiency 25C	ALPHA	0.060	0.040
8	Weighted comb. of leaf reflectances VIS	ALPHA_vl	0.11	0.11
9	Weighted comb. of leaf reflectances NIR	ALPHA_nl	0.35	0.35
10	Weighted comb. of stem reflectances VIS	ALPHA_vs	0.31	0.31
11	Weighted comb. of stem reflectances NIR	ALPHA_ns	0.53	0.53
12	Weighted comb. of leaf transmittances VIS	TETA_vl	0.050	0.050
13	Weighted comb. of leaf transmittances NIR	TETA_nl	0.34	0.34
14	Weighted comb. of stem transmittances VIS	TETA_vs	0.12	0.12
15	Weighted comb. of stem transmittances NIR	TETA_ns	0.25	0.25
16	Departure of leaf angles from a random distribution equals	X_l	-0.30	-0.30
17	Rooting distribution parameter	ROOTA_PAR	11.0	11.0
18	Rooting distribution parameter	ROOTB_PAR	2.0	2.0
19	Value for SLA at the top of canopy	SLA_o	0.030	0.030
20	Linear slope coefficient	SLA_m	0.0	0.0
21	Leaf carbon to nitrogen ratio (leaf C:N)	CN_L	25.0	25.0
22	Fraction of leaf nitrogen in Rubisco	F_LNR	0.090	0.090
23	Soil water potential when stomata fully open	PSI_o	-0.74e5,	-0.74e5
24	Soil water potential when stomata fully close	PSI_c	-2.75e5,	-2.75e5
25	Nitrogen availability factor	F_N	0.61	0.64
26	Binary flag for woody lifeform: 1. = woody, 0. = not woody	WOODY	0.0	0.0
27	Leaf litter C:N	LF_LIT_CN	50.0	50.0
28	Fine root C:N	F_ROOT_CN	42.0	42.0
29	Live wood C:N	LIVEWD_CN	0.0	0.0
30	Dead wood C:N	DEADWD_CN	0.0	0.0
31	Allocation parameter: new fine root C per new leaf C	F_ROOT_LEAF	3.0	3.0

Table 3: PFT parameteres - Part 1

	Parameter	Model name	PFT plant types	
			C3 grass	C4 grass
32	Allocation parameter: new stem c per new leaf C	STEM_LEAF	0.0	0.0
33	Allocation parameter: new coarse root C per new stem C	C_ROOT_STEM	0.0	0.0
34	Fraction of new wood that is live	F_LIVE_WD	0.0	0.0
35	Fraction of allocation that goes to currently displayed growth, remainder to storage	F_CUR	0.5	0.5
36	Fraction of leaf litter labile	LF_FLAB	0.25	0.25
37	Fraction of leaf litter cellulose	LF_FCEL	0.50	0.50
38	Fraction of leaf litter lignin	LF_FLIG	0.25	0.25
39	Fraction of fine root litter labile	FR_FLAB	0.25	0.25
40	Fraction of fine root litter cellulose	FR_FCEL	0.50	0.50
41	Fraction of fine root litter lignin	FR_FLIG	0.25	0.25
42	Fraction of dead wood cellulose	DW_FCEL	0.75	0.75
43	Fraction of dead wood lignin	DW_FLIG	0.25	0.25
44	Leaf longevity (yrs)	LEAF_LONG	1.0	1.0
45	Binary flag for evergreen leaf habit	EVERGREEN	0.0	0.0
46	Binary flag for stress-deciduous leaf habit	STRESS_DECID	1.0	1.0
47	Binary flag for seasonal-deciduous leaf habit	SEASON_DECID	0.0	0.0
48	Fire resistance index (unitless)	RESIST	0.12	0.12

Table 4: PFT parameteres - Part 2
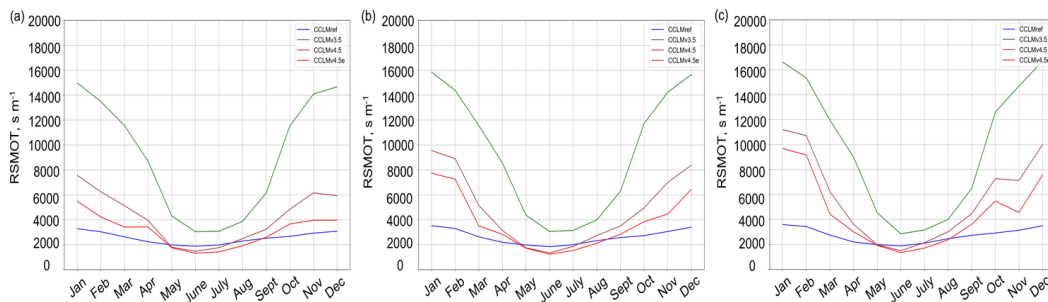
11.2 Additional figures - Parc domain:

Figure 13: Mean seasonal cycle of stomatal resistance for Parc (**a**), Linden (**b**) and Lindenberg (**c**) domains based on monthly values. Climatological means for CCLMref (blue line), CCLMv3.5 (green line), CCLMv4.5 (brown line) and CCLMv4.5e (red line) are calculated for the period 2010-2015.
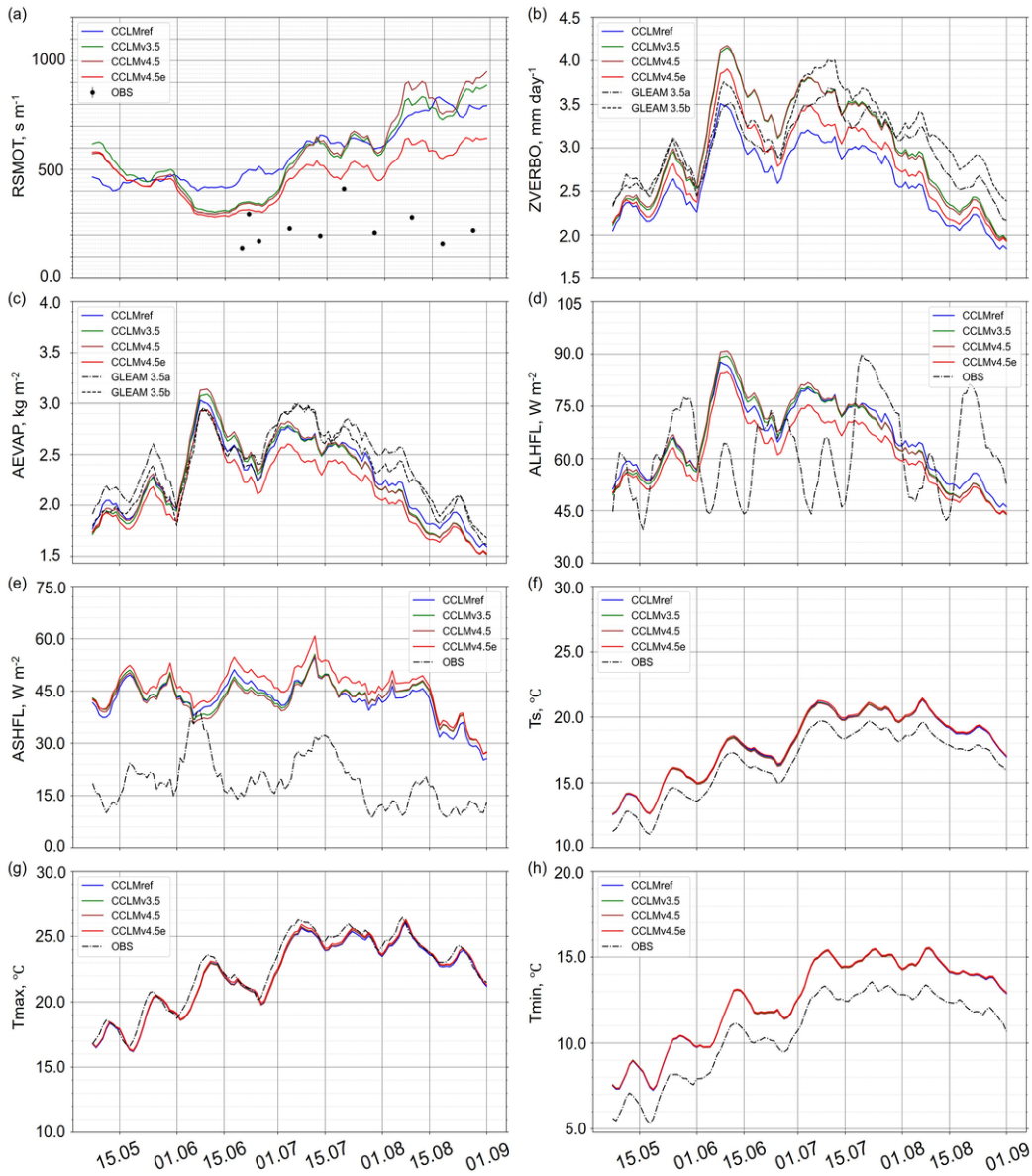
11.3 Additional figures - Linden domain:

Figure 14: Daily mean stomatal resistance (**a**), total evaporation (**b**), the amount of water evaporation (**c**), latent (**d**) and sensible (**e**) heat fluxes, near-surface (**f**), maximum (**g**) and minimum (**h**) air temperatures at the Linden domain averaged over the period 2010-2015: CCLMref (blue), CCLMv3.5 (green), CCLMv4.5 (brown), CCLMv4.5e (red).
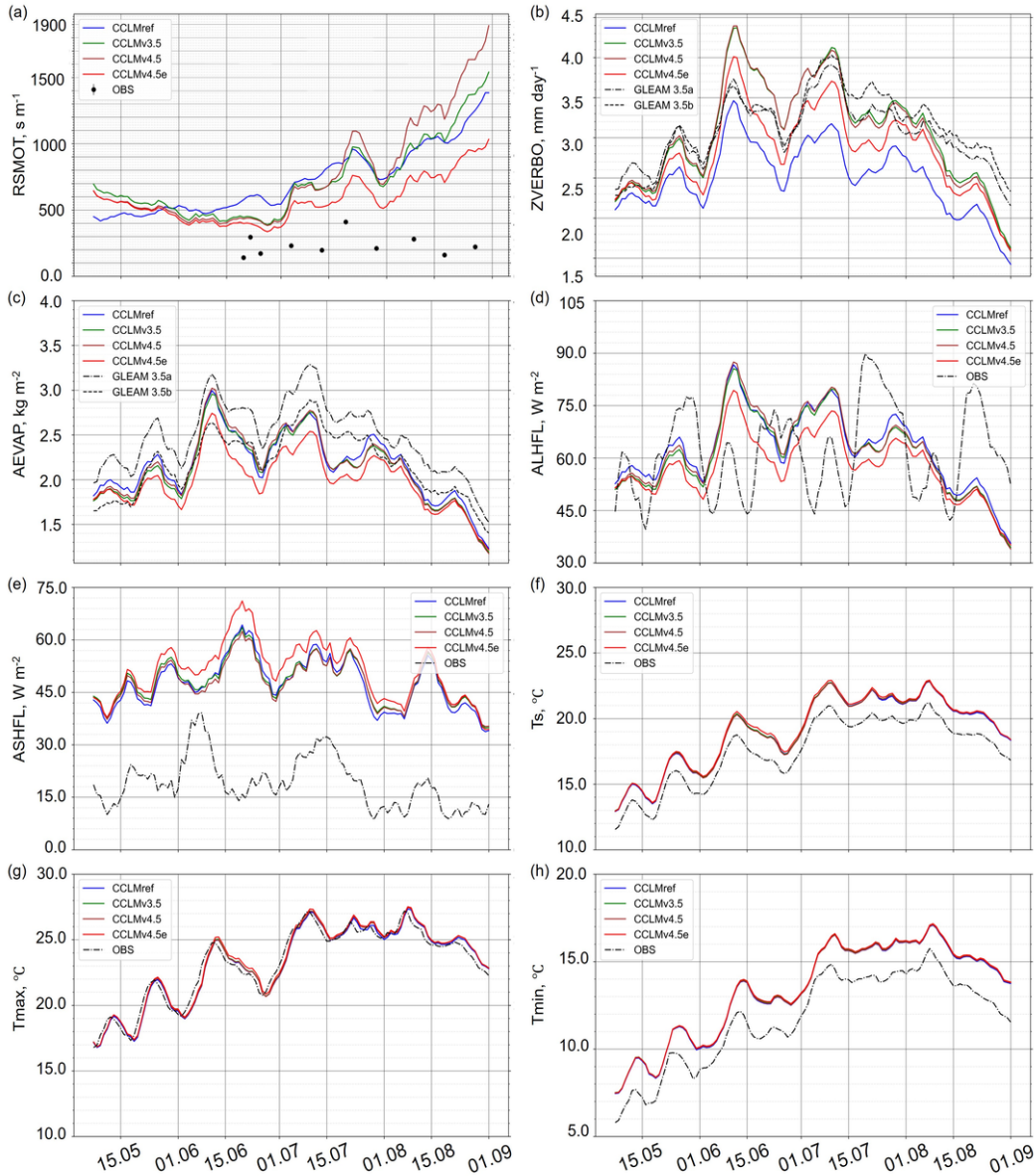
11.4   Additional figures - Lindenberg domain:

Figure 15: Daily mean stomatal resistance (**a**), total evaporation (**b**), the amount of water evaporation (**c**), latent (**d**) and sensible (**e**) heat fluxes, near-surface (**f**), maximum (**g**) and minimum (**h**) air temperatures at the Lindenberg domain averaged over the period 2010-2015: CCLMref (blue), CCLMv3.5 (green), CCLMv4.5 (brown), CCLMv4.5e (red).

12   Meetings

- 22nd COSMO General Meeting, 1-11 September 2020, teleconferences;

- ICCARUS (ICON/COSMO/CLM/ART USER Seminar) 2021, virtual seminar 8 - 19 March 2021;

- PT VAINT virtual meeting;

- 23rd COSMO General Meeting, 14-17 September 2021, teleconference;

- ICCARUS (ICON/COSMO/CLM/ART USER Seminar) 2022, virtual seminar 7 - 11 March 2022;

13   Presentations

- Introduction to PT VAINT;

- PT˙VAINT - current status;

- PT˙VAINT - changes and results;

- PT˙VAIN - latest news about priority task;

- PT˙VAINT - extreme events and dynamic LAI tests;

14   Code and data availability

The new vegetation algorithms are fully implemented in COSMO-CLM v6.0. The model code is available:
`https://github.com/COSMO-ORG/cosmo/tree/cosmo_clm6.0_phenology`. The latest version of scripts which were created and applied for this research are available as a Python packages from `https://github.com/EvgenyChur/PT-VAINT` and
`https://github.com/EvgenyChur/CESR` under the GPLv3 license.

15   Acknowledgments

16   Financial support

17   References

Arakawa, A. and Lamb, V.R., 1977. Computational design of the basic dynamical processes of the UCLA general circulation model. *Methods in Computational Physics: Advances in Research and Applications* **17**, 173–265.
`https://doi.org/10.1016/B978-0-12-460817-7.50009-4`

Arora, V. K., 2002. Modeling vegetation as a dynamic component in soil-vegetation-atmosphere transfer schemes and hydrological models. *Reviews of Geophysics* **2**, 1–26. https://doi.org/10.1029/2001RG000103

Ball, J.T. and Berry, J.A., 1991. An analysis and concise description of stomatal responses to multiple environmental factors *Planta*

Ball, J.T., Woodrow, I. E. and Berry, J. A., 1987. A Model Predicting Stomatal Conductance and Its Contribution to the Control of Photosynthesis Under Different Environmental Conditions. In: *Progress in Photosynthesis Research,* (eds. J. Biggins), Springer, Dordrecht, 221–224. https://doi.org/10.1007/978-94-017-0519-6_48

Ball, J. T., 1988. An Analysis of Stomatal Conductance. *Ph.D. thesis* Stanford University, USA, 89 pp.

Berry, J.A., Beerling, D.J. and Franks, P.J., 2010. Stomata: key players in the earth system, past and present. *Plant Biology* **13**, 232–239. https://doi.org/10.1016/j.pbi.2010.04.013

Betts, A.K., Ball, J.H., Beljaars, A.C.M., Miller, M.J. and Viterbo, V., 1996. The land-surface-atmosphere interaction: a review based on observational and global modeling perspectives. *J. Geophys. Res.* **101**, 7209–7225. https://doi.org/10.1029/95JD02135

Beyrich, F., and Adam, W.K., 2007. Site and Data Report for Lindenberg Reference Site in CEOP Phase 1 *Data Report No. 230*, Deutscher Wetterdienst, Offenbach am Main, 55p.

Bogena, H.R. and TERENO team., 2018. The TERENO-Rur Hydrological Observatory: A Multiscale Multi-Compartment Research Platform for the Advancement of Hydrological Science. *Vadose Zone J.* **17(1)**, 1–22. https://doi.org/10.2136/vzj2018.03.0055

Bonan, G. B., 1996. A Land Surface model (LSM version 1.0) for Ecological, Hydrological, and Atmospheric Studies: Technical Description and Users Guide. *Technical Note* Boulder, Colorado, 150 pp.

Bonan, G.B. and Levis, S., 2002. Landscapes as patches of plant functional types: An integrating concept for climate and ecosystem models. *Glob. Biogeochem. Cycles* **16(2)**, 1021–1051. https://doi.org/10.1029/2000gb001360

Bruns, E., Chmielewski, F-M. and van Vliet A.J.H., 2003. The global phenological monitoring concept. In: *Phenology,* (eds. M.D. Schwartz), Springer, Dordrecht, 93–104. https://doi.org/10.1007/978-94-007-0632-3_7

Calvet, J.C., Noilhan, J., Roujean, J.L., Bessemoulin, P., Cabelguenne, M., Olioso, A. and Wigneron, J.P., 1998. An interactive vegetation svat model tested against data from six contrasting sites. *Agric. and For. Meteorol.* **92(2)**, 73–95.

Calvet, J.C., Rivalland, V., Picon-Cochard, C. and Guehl, J. M., 2004. Modelling forest transpiration and co2 fluxes - response to soil moisture stress. *Agric. and For. Meteorol.* **124(3-4)**, 143–156. https://doi.org/10.1016/j.agrformet.2004.01.007

Calvet, J.C., Gibelin, A.L., Roujean, J.L., Martin, E., Le Moigne, P., Douville, H. and Noilhan. J., 2008. Past and future scenarios of the effect of carbon dioxide on plant growth and transpiration for three vegetation types of southwestern france. *Atmos. Chem. and*

Phys. **8(2)**, 397–406. https://doi.org/10.5194/acp-8-397-2008

Clapp, R.B. and Hornberger, G.M., 1978. Empirical equations for some soil hydraulic properties. *Water Resour. Res.* **14(4)**, 601–604.
https://doi.org/10.1029/WR014i004p00601

Collatz, G.J., Ball, J.T., Grivet, C. and Berry, J. A., 1991. Physiological and environmental regulation of stomatal conductance, photosynthesis and transpiration: a model that includes a laminar boundary layer. *Agric. For. Meteorol.* **54(4)**, 107–136.
https://doi.org/10.1016/0168-1923(91)90002-8

Dai, Y. and Zeng, Q., 1997. A land surface model (IAP94) for climate studies, Part I: Formulation and validation in off-line experiments. *Adv. Atmos. Sci.* **14**, 443–460.
https://doi.org/10.1007/s00376-997-0063-4

Dai, Y., Dickinson, R.E. and Wang, Y.P., 2004. A two-big-leaf model for canopy temperature, photosynthesis, and stomatal conductance. *J. Clim.* **17**, 2281–2299.
https://doi.org/10.1175/1520-0442(2004)017<2281:ATMFCT>2.0.CO;2

Davin, E.L. and Seneviratne, S.I. 2012. Role of land surface processes and diffuse/direct radiation partitioning in simulating the European climate. *Biogeosciences* **9**, 1695–1707.
https://doi.org/10.5194/bg-9-1695-2012

Davin, E.L., Stoeckli, R., Jaeger, E.B., Levis, S. and Seneviratne, S.I., 2011. COSMO-CLM2: A new version of the COSMO-CLM model coupled to the Community Land Model. *Clim. Dyn.* **37(9)**, 1889–1907. https://doi.org/10.1007/s00382-011-1019-z

de Noblet-Ducoudre, N. and Pitman, A., 2021. Terrestrial processes and their roles in climate change. *Oxford Research Encyclopedia of Climate Science*, 1–27.
https://doi.org/10.1093/acrefore/9780190228620.013.825

Dickinson, R.E., Kennedy, P.J. and Sellers, H.A., 1993. Biosphere-Atmosphere Transfer Scheme (BATS) version 1e as coupled to the NCAR Community Climate Model. *Technical report* National Centre for Atmospheric Research (NCAR), Boulder, CO (United States). Climate and Global Dynamics Division., 80 pp.

Dokuchaev, V., 1899. The doctrine of the zones of nature: horizontal and vertical soil zones. St. Petersburg.

Doms, G., Frstner, J., Heise, E., Herzog, H.-J., Mironov, D., Raschendorfer, M., Reinhardt, T., Ritter, B., Schrodin, R., Schulz, J.-P. and Vogel, G., 2018. A description of the Nonhydrostatic Regional COSMO Model Part II: Physical Parameterization. *Deutscher Wetterdienst* Offenbach, Germany, 167pp., 2018.

Everwand, G, Fry, EL, Eggers, T., and Manning, P., 2014. Seasonal variation in the relationship between plant traits and grassland carbon and water fluxes. *Ecosystems* **17**, 1095–1108.
https://doi.org/10.1007/s10021-014-9779-z

Farquhar, G.D., von Caemmerer, S. and Berry, J.A. 1980. A biochemical model of photosynthetic CO2 assimilation in leaves of C3 species. *Planta* **149**, 78–90.
https://doi.org/10.1007/BF00386231

Frick, C., Steiner, H., Mazurkiewicz, A., Riediger, U., Rauthe, M., Reich, T. and Gratzki, A., 2014. Central European high-resolution gridded daily data sets (HYRAS): Mean temperature and relative humidity. *Meteorol. Z.* **23**, 15–32.
`https://doi.org/10.1127/0941-2948/2014/0560`

Gibelin, A.L., Calvet, J.C. and Viovy, N., 2008. Modelling energy and CO_2 fluxes with an interactive vegetation land surface model-evaluation at high and middle latitudes. *Agric. and For. Meteorol.* **148(10)**, 1611–1628.
`https://doi.org/10.1016/j.agrformet.2008.05.013`

Goudriaan, J., van Laar, H.H., van Keulen, W. and Louwerse, W., 1985. Photosynthesis, CO2 and plant production. In: *Wheat growth and modelling,* (eds. W. Day and R.K. Atkin), Plenum Press, New York, 107–122. `https://edepot.wur.nl/217653`

Jacobs, C.M.J., 1994. Direct impact of CO_2 enrichment on regional transpiration. *PhD thesis* Agricultural University, Wageningen, The Netherlands, 193pp.

Jarvis, P. G., 1976 The interpretation of the variations in leaf water potential and stomatal conductance found in canopies in the field. *Biological Sciences* **273(927)**, 593–610.
`https://doi.org/10.1098/rstb.1976.0035`

Jarvis, A. J. and Davies, W.J., 1998. The coupled response of stomatal conductance to photosynthesis and transpiratio. *J. Exp. Bot.* **49**, 399–406.
`https://www.jstor.org/stable/23695973`

Jasechko, S., Sharp, Z.D., Gibson, J.J., Birks, S. J. and Fawcett, P. J., 2013. Terrestrial water fluxes dominated by transpiration. *Nature* **496**, 347–350.
`https://doi.org/10.1038/nature11983`

Kattge, J. and TRY team., 2019: . TRY plant trait database - enhanced coverage and open access. *Glob. Change Biol.* **26(1)**, 119–188. `https://doi.org/10.1111/gcb.14904`

Kaufmann, M.R. and Thor, G.L., 1982. Measurement of water stress in subalpine trees: effects of temporary tissue storage methods and needle age. *Can. J. For. Res.* **12(4)**, 969–972. `https://doi.org/10.1139/x82-138`

Koster, R.D., Dirmeyer, P.A., Hahmann, A.N., Ijpelaar, R., Tyahla, L., Cox, P. and Suarez, M.J., 2002. Comparing the degree of landatmosphere interaction in four atmospheric general circulation models. *J. Hydrometeorol.* **3(3)**, 363–375.
`https://doi.org/10.1175/1525-7541(2002)003<0363:CTDOLA>2.0.CO;2`

Le Moigne, P, 2018. SURFEX scientific documentation. *Technical report* **MeteoFrance**, 304pp.

Luo, X., Chen, J. M., Liu, J., Black, T.A., Croft, H., Staebler, R., He, L., Arain, A., Chen, B., Mo, G., Gonsamo, A. and McCaughey, H., 2018. Comparison of big-leaf, two-big-leaf, and two-leaf upscaling schemes for evapotranspiration estimation using coupled carbon-water modeling. *J. Geophys. Res. Biogeosci.* **123**, 207–225.
`https://doi.org/10.1002/2017JG003978`

Mahfouf, J. F. and Noilhan, J., 1996. Inclusion of gravitational drainage in a land surface scheme based on the force-restore method. *J. Appl. Meteorol.* **35(6)**, 987–992.

https://doi.org/10.1175/1520-0450(1996)035<0987:IOGDIA>2.0.CO;2

Maire, V. and team, 2016. Data from: Global effects of soil and climate on leaf photosynthetic traits and rates (dataset). *Dataset* https://doi.org/10.5061/dryad.j42m7

Martens, B., Miralles, D.G., Lievens, H., van der Schalie, R., de Jeu, R.A.M., Fernndez-Prieto, D., Beck, H.E., Dorigo, W.A., and Verhoest, N.E.C., 2017. GLEAM v3: Satellite-based land evaporation and root-zone soil moisture. *GMD* **10(5)**, 1903–1925. https://doi.org/10.5194/gmd-10-1903-2017

Matheny, A.M. and team., 2014. Characterizing the diurnal patterns of errors in the prediction of evapotranspiration by several land-surface models: An NACP analysis. *Biogeosciences* **19(7)**, 1458–1473. https://doi.org/10.1002/2014JG002623

Monteith, J.L. and Unsworth, M.H., 1990. Principles of Environmental. *Physics. 2nd Edition* Butterworth-Heinemann, Elsevier, Oxford, 422p.

Nogueira, M., Albergel, A., Boussetta, S., Johannsen, F., Trigo, I.F., Ermida, S.L., Martins, J.P.A., and Dutra, E., 2020. Role of vegetation in representing land surface temperature in the CHTESSEL (CY45R1) and SURFEX-ISBA (v8.1) land surface models: a case study over Iberia. *GMD* **13**, 3975–3993. https://doi.org/10.5194/gmd-13-3975-2020

Oleson, K.W. and CLM team,, 2010. Technical Description of version 4.0 of the Community Land Model (CLM). *Technical report* National Centre for Atmospheric Research (NCAR), Boulder, CO (United States). Climate and Global Dynamics Division., 266 pp.

Oleson, K.W. and CLM team., 2013. Technical Description of version 4.5 of the Community Land Model (CLM). *Technical report* National Centre for Atmospheric Research (NCAR), Boulder, CO (United States). Climate and Global Dynamics Division., 434 pp.

Osborn, T.J. and Hulme, M., 1998. Evaluation of the European daily precipitation characteristics from the Atmospheric Model Intercomparison Project. *Int. J. Climate.* **18**, 505–522. https://doi.org/10.1002/(SICI)1097-0088(199804)18:5<505::AID-JOC263>3.0.CO;2-7

Regenass, D., Schlemmer, L., Fuhrer, O., Bettems, J-M., Arpagaus, M. and Schaer, C., 2021. Validation of a High-Resolution Numerical Weather Prediction Land Surface Scheme Using Catchment Water Balances. *J. Hydrometeorol.* **22**, 3189–3210. https://doi.org/10.1175/JHM-D-20-0273.1

Ritter, B. and Geleyn, J.F., 1992. A comprehensive radiation scheme for numerical weather prediction models with potential applications in climate simulations. *Mon. Weather Rev.* **120**, 303–325. https://doi.org/10.1175/1520-0493(1992)120<0303:ACRSFN>2.0.CO;2

Rockel, B., Will, A. and Hence, A., 2008. The Regional Climate Model COSMO-CLM (CCLM). *Meteorol. Z.* **17(4)**, 347–348. https://doi.org/10.1127/0941-2948/2008/0309

Ryan, M., 1991. Effects of Climate Change on Plant Respiration. *Ecological Applications* **1**, 157–167. https://doi.org/10.2307/1941808

Schaer, C., Vidale, P.L., Lthi, D., Frei, C., Hberli, C., Liniger, M.A. and Appenzeller, C., 2004. The role of increasing temperature variability in European summer heatwaves. *Nature*

427, 332–336. `https://doi.org/10.1038/nature02300`

Schrodin, E., and Heise, E., 2002. A New Multi-Layer Soil Model. *COSMO Newsletter* **2**, 149–151.

Schroeder-Georgi, T., Wirth, C., Nadrowski, K., Meyer, S. T., Mommer, L. and Weigelt, A., 2016. From pots to plots: hierarchical trait-based prediction of plant performance in a mesic grassland. *J. Ecol* **104**, 206–218. `https://doi.org/10.1111/1365-2745.12489`

Schulz, J.P., and Vogel, G., 2020. Improving the processes in the land surface scheme TERRA: bare soil evaporation and skin temperature. *Atmosphere* **11**, 513–530. `https://doi.org/10.3390/atmos11050513`

Schulz, J.P., Vogel, G. and Ahrens, B., 2015. A new leaf phenology for the land surface scheme TERRA of the COSMO atmospheric model. *COSMO Newsletter* **15**, 21–29.

Sellers, P.J., Randall, D.A., Collatz, G.J., Berry, J.A., Field, C.B., Dazlich, D.A., Zhang, C., Collelo, G.D. and Bounoua, L., 1996. A revised land surface parameterisation (SiB2) for atmospheric GCMs. Part I: Model formulation. *J. Climate* **9**, 676–705. `https://doi.org/10.1175/1520-0442(1996)009<0676:ARLSPF>2.0.CO;2`

Shrestha, P. and Simmer, C., 2020. Modeled Land Atmosphere Coupling Response to Soil Moisture Changes with Different Generations of Land Surface Models. *Water* **12**, 46–62. `https://doi.org/10.3390/w12010046`

Stoeckli, R., Rutishauser, T., Dragoni, D., OKeefe, J., Thornton, P.E., Jolly, M., Lu, I. and Denning, A.S., 2008. Remote sensing data assimilation for a prognostic phenology model. *J. Geophys. Res.* **113**, 1–19. `https://doi.org/10.1029/2008JG000781`

Thornton, P. E. and Zimmermann, N. E., 2007. An improved canopy integration scheme for a Land Surface Model with prognostic canopy structure. *J. Clim.* **20(15)**, 3902–3923. `https://doi.org/10.1175/JCLI4222.1`

Toelle, H. M., Gutjahr, O., Busch, G. and Thiele, J.C., 2014. Increasing bioenergy production on arable land: Does the regional and local climate respond? Germany as a case study. *J. Geophys. Res.* **119(6)**, 2711–2724. `https://doi.org/10.1002/2013JD020877`

Toelle, M.H. and Churiulin, E., 2021. . Climate uncertainty due to different land cover maps in convection-permitting regional climate simulations: role of land surface characteristics for temperature and climate extremes. *Front. Earth Sci. - Atmospheric Science* **9**, 954–976. `https://doi.org/10.3389/feart.2021.722244`

Uebel, M., 2015. Simulation of mesoscale patterns and diurnal variations of atmospheric CO2 mixing ratios with the model system TERRSYSMP-CO2, *Ph.D. thesis* Meteorologisches Insitut der Universitt Bonn, Germany, 176 pp.

van den Broeke, M.S., Kalin, A., Alavez, J.A.T., Oglesby, R. and Hu. Q., 2018. A warm-season comparison of WRF coupled to the CLM4.0., Noah-MP, and Bucket hydrology land surface schemes over the central USA. *Theor. Appl. Climatol.* **134**, 801–816. `https://doi.org/10.1007/s00704-017-2301-8`

Wang, Y.P. and Leuning, R., 1998. A two-leaf model for canopy conductance, photosynthesis

and partitioning of available energy. I. Model description and comparison with a multi-layered model. *Agric. For. Meteorol.* **91**, 89–111.
https://doi.org/10.1016/S0168-1923(98)00061-6

Wicker, L.J., and Skamarock, W.C., 2004. Time-splitting methods for elastic models using forward time schemes. *Mon. Weather Rev.* **130**, 2088–2097.
https://doi.org/10.1175/1520-0493(2002)130<2088:TSMFEM>2.0.CO;2

Wicker, L.J. and Skamarock, W.C., 2002. Time-splitting methods for elastic models using forward time schemes. *Mon. Weather Rev.* **130(8)**, 2088–2097.
https://doi.org/10.1175/1520-0493(2002)130<2088:TSMFEM>2.0.CO;2

Wu, Y., Liu, S. and Abdul-Aziz, O.I., 2012. Hydrological effects of the increased CO2 and climate change in the Upper Mississippi River Basin using a modified SWAT. *Clim. Change* **110**, 977–1003. https://doi.org/10.1007/s10584-011-0087-8

List of COSMO Newsletters and Technical Reports

(available for download from the COSMO Website: www.cosmo-model.org)

COSMO Newsletters

No. 1: February 2001.

No. 2: February 2002.

No. 3: February 2003.

No. 4: February 2004.

No. 5: April 2005.

No. 6: July 2006.

No. 7: April 2008; Proceedings from the 8th COSMO General Meeting in Bucharest, 2006.

No. 8: September 2008; Proceedings from the 9th COSMO General Meeting in Athens, 2007.

No. 9: December 2008.

No. 10: March 2010.

No. 11: April 2011.

No. 12: April 2012.

No. 13: April 2013.

No. 14: April 2014.

No. 15: July 2015.

No. 16: July 2016.

No. 17: July 2017.

No. 18: November 2018.

No. 19: October 2019.

No. 20: December 2020.

COSMO Technical Reports

No. 1: Dmitrii Mironov and Matthias Raschendorfer (2001):
Evaluation of Empirical Parameters of the New LM Surface-Layer Parameterization Scheme. Results from Numerical Experiments Including the Soil Moisture Analysis.

No. 2: Reinhold Schrodin and Erdmann Heise (2001):
The Multi-Layer Version of the DWD Soil Model TERRA_LM.

No. 3: Günther Doms (2001):
A Scheme for Monotonic Numerical Diffusion in the LM.

No. 4: Hans-Joachim Herzog, Ursula Schubert, Gerd Vogel, Adelheid Fiedler and Roswitha Kirchner (2002):
LLM ¯ the High-Resolving Nonhydrostatic Simulation Model in the DWD-Project LIT-FASS.
Part I: Modelling Technique and Simulation Method.

No. 5: Jean-Marie Bettems (2002):
EUCOS Impact Study Using the Limited-Area Non-Hydrostatic NWP Model in Operational Use at MeteoSwiss.

No. 6: Heinz-Werner Bitzer and Jürgen Steppeler (2004):
Documentation of the Z-Coordinate Dynamical Core of LM.

No. 7: Hans-Joachim Herzog, Almut Gassmann (2005):
Lorenz- and Charney-Phillips vertical grid experimentation using a compressible non-hydrostatic toy-model relevant to the fast-mode part of the 'Lokal-Modell'.

No. 8: Chiara Marsigli, Andrea Montani, Tiziana Paccagnella, Davide Sacchetti, André Walser, Marco Arpagaus, Thomas Schumann (2005):
Evaluation of the Performance of the COSMO-LEPS System.

No. 9: Erdmann Heise, Bodo Ritter, Reinhold Schrodin (2006):
Operational Implementation of the Multilayer Soil Model.

No. 10: M.D. Tsyrulnikov (2007):
Is the particle filtering approach appropriate for meso-scale data assimilation ?

No. 11: Dmitrii V. Mironov (2008):
Parameterization of Lakes in Numerical Weather Prediction. Description of a Lake Model.

No. 12: Adriano Raspanti (2009):
COSMO Priority Project "VERification System Unified Survey" (VERSUS): Final Report.

No. 13: Chiara Marsigli (2009):
COSMO Priority Project "Short Range Ensemble Prediction System" (SREPS): Final Report.

No. 14: Michael Baldauf (2009):
COSMO Priority Project "Further Developments of the Runge-Kutta Time Integration Scheme" (RK): Final Report.

No. 15: Silke Dierer (2009):
COSMO Priority Project "Tackle deficiencies in quantitative precipitation forecast" (QPF): Final Report.

No. 16: Pierre Eckert (2009):
COSMO Priority Project "INTERP": Final Report.

No. 17: D. Leuenberger, M. Stoll and A. Roches (2010):
Description of some convective indices implemented in the COSMO model.

No. 18: Daniel Leuenberger (2010):
Statistical analysis of high-resolution COSMO Ensemble forecasts in view of Data Assimilation.

No. 19: A. Montani, D. Cesari, C. Marsigli, T. Paccagnella (2010):
Seven years of activity in the field of mesoscale ensemble forecasting by the COSMO–LEPS system: main achievements and open challenges.

No. 20: A. Roches, O. Fuhrer (2012):
Tracer module in the COSMO model.

No. 21: Michael Baldauf (2013):
A new fast-waves solver for the Runge-Kutta dynamical core.
DOI: 10.5676/DWD_pub/nwv/cosmo-tr_21

No. 22: C. Marsigli, T. Diomede, A. Montani, T. Paccagnella, P. Louka, F. Gofa, A. Corigliano (2013):
The CONSENS Priority Project.
DOI: 10.5676/DWD_pub/nwv/cosmo-tr_22

No. 23: M. Baldauf, O. Fuhrer, M. J. Kurowski, G. de Morsier, M. Müllner, Z. P. Piotrowski, B. Rosa, P. L. Vitagliano, D. Wójcik, M. Ziemiański (2013):
The COSMO Priority Project 'Conservative Dynamical Core' Final Report.
DOI: 10.5676/DWD_pub/nwv/cosmo-tr_23

No. 24: A. K. Miltenberger, A. Roches, S. Pfahl, H. Wernli (2014):
Online Trajectory Module in COSMO: a short user guide.
DOI: 10.5676/DWD_pub/nwv/cosmo-tr_24

No. 25: P. Khain, I. Carmona, A. Voudouri, E. Avgoustoglou, J.-M. Bettems, F. Grazzini (2015):
The Proof of the Parameters Calibration Method: CALMO Progress Report.
DOI: 10.5676/DWD_pub/nwv/cosmo-tr_25

No. 26: D. Mironov, E. Machulskaya, B. Szintai, M. Raschendorfer, V. Perov, M. Chumakov, E. Avgoustoglou (2015):
The COSMO Priority Project 'UTCS' Final Report.
DOI: 10.5676/DWD_pub/nwv/cosmo-tr_26

No. 27: J-M. Bettems (2015):
The COSMO Priority Project 'COLOBOC': Final Report.
DOI: 10.5676/DWD_pub/nwv/cosmo-tr_27

No. 28: Ulrich Blahak (2016):
RADAR_MIE_LM and RADAR_MIELIB - Calculation of Radar Reflectivity from Model Output.
DOI: 10.5676/DWD_pub/nwv/cosmo-tr_28

No. 29: M. Tsyrulnikov and D. Gayfulin (2016):
A Stochastic Pattern Generator for ensemble applications.
DOI: 10.5676/DWD_pub/nwv/cosmo-tr_29

No. 30: D. Mironov and E. Machulskaya (2017):
A Turbulence Kinetic Energy – Scalar Variance Turbulence Parameterization Scheme.
DOI: 10.5676/DWD_pub/nwv/cosmo-tr_30

No. 31: P. Khain, I. Carmona, A. Voudouri, E. Avgoustoglou, J.-M. Bettems, F. Grazzini, P. Kaufmann (2017):
CALMO - Progress Report.
DOI: 10.5676/DWD_pub/nwv/cosmo-tr_31

No. 32: A. Voudouri, P. Khain, I. Carmona, E. Avgoustoglou, J.M. Bettems, F. Grazzini, O. Bellprat, P. Kaufmann and E. Bucchignani (2017):
Calibration of COSMO Model, Priority Project CALMO Final report.
DOI: 10.5676/DWD_pub/nwv/cosmo-tr_32

No. 33: N. Vela (2017):
VAST 2.0 - User Manual.
DOI: 10.5676/DWD_pub/nwv/cosmo-tr_33

No. 34: C. Marsigli, D. Alferov, M. Arpagaus, E. Astakhova, R. Bonanno, G. Duniec, C. Gebhardt, W. Interewicz, N. Loglisci, A. Mazur, V. Maurer, A. Montani, A. Walser (2018):
COsmo Towards Ensembles at the Km-scale IN Our countries (COTEKINO), Priority Project final report.
DOI: 10.5676/DWD_pub/nwv/cosmo-tr_34

No. 35: G. Rivin, I. Rozinkina, E. Astakhova, A. Montani, D. Alferov, M. Arpagaus, D. Blinov, A. Bundel, M. Chumakov, P. Eckert, A. Euripides, J. Förstner, J. Helmert, E. Kazakova, A. Kirsanov, V. Kopeikin, E. Kukanova, D. Majewski, C. Marsigli, G. de Morsier, A. Muravev, T. Paccagnella, U. Schättler, C. Schraff, M. Shatunova, A. Shcherbakov, P. Steiner, M. Zaichenko (2018):
The COSMO Priority Project CORSO Final Report.
DOI: 10.5676/DWD_pub/nwv/cosmo-tr_35

No. 36: A. Raspanti, A. Celozzi, A. Troisi, A. Vocino, R. Bove, F. Batignani (2018):
The COSMO Priority Project VERSUS2 Final Report.
DOI: 10.5676/DWD_pub/nwv/cosmo-tr_36

No. 37: A. Bundel, F. Gofa, D. Alferov, E. Astakhova, P. Baumann, D. Boucouvala, U. Damrath, P. Eckert, A. Kirsanov, X. Lapillonne, J. Linkowska, C. Marsigli, A. Montani, A. Muraviev, E. Oberto, M.S. Tesini, N. Vela, A. Wyszogrodzki, M. Zaichenko, A. Walser (2019):
The COSMO Priority Project INSPECT Final Report.
DOI: 10.5676/DWD_pub/nwv/cosmo-tr_37

No. 38: G. Rivin, I. Rozinkina, E. Astakhova, A. Montani, J-M. Bettems, D. Alferov, D. Blinov, P. Eckert, A. Euripides, J. Helmert, M.Shatunova (2019):
The COSMO Priority Project CORSO-A Final Report.
DOI: 10.5676/DWD_pub/nwv/cosmo-tr_38

No. 39: C. Marsigli, D. Alferov, E. Astakhova, G. Duniec, D. Gayfulin, C. Gebhardt, W. Interewicz, N. Loglisci, F. Marcucci, A. Mazur, A. Montani, M. Tsyrulnikov, A. Walser (2019):
Studying perturbations for the representation of modeling uncertainties in Ensemble development (SPRED Priority Project): Final Report.
DOI: 10.5676/DWD_pub/nwv/cosmo-tr_39

No. 40: E. Bucchignani, P. Mercogliano, V. Garbero, M. Milelli, M. Varentsov, I. Rozinkina, G. Rivin, D. Blinov, A. Kirsanov, H. Wouters, J.-P. Schulz, U. Schättler (2019):

Analysis and Evaluation of TERRA_URB Scheme: PT AEVUS Final Report.
DOI: 10.5676/DWD_pub/nwv/cosmo-tr_40

No. 41: X. Lapillonne, O. Fuhrer (2020):
Performance On Massively Parallel Architectures (POMPA): Final report.
DOI: 10.5676/DWD_pub/nwv/cosmo-tr_41

No. 42: E. Avgoustoglou, A. Voudouri, I Carmona, E. Bucchignani, Y. Levy, J. -M. Bettems (2020):
A methodology towards the hierarchy of COSMO parameter calibration tests via the domain sensitivity over the Mediterranean area.
DOI: 10.5676/DWD_pub/nwv/cosmo-tr_42

No. 43: H. Muskatel, U. Blahak, P. Khain, A. Shtivelman, M. Raschendorfer, M. Kohler, D. Rieger, O. Fuhrer, X. Lapillonne, G. Rivin, N. Chubarova, M. Shatunova, A. Poliukhov, A. Kirsanov, T. Andreadis, S. Gruber (2021):
The COSMO Priority Project $T^2(RC)^2$: Testing and Tuning of Revised Cloud Radiation Coupling, Final Report
DOI: 10.5676/DWD_pub/nwv/cosmo-tr_43

No. 44: M. Baldauf, D. Wojcik, F. Prill, D. Reinert, R. Dumitrache, A. Iriza, G. deMorsier, M. Shatunova, G. Zaengl, U. Schaettler (2021):
The COSMO Priority Project CDIC: Comparison of the dynamical cores of ICON and COSMO, Final Report
DOI: 10.5676/DWD_pub/nwv/cosmo-tr_44

COSMO Technical Reports

Issues of the COSMO Technical Reports series are published by the *COnsortium for Small-scale MOdelling* at non-regular intervals. COSMO is a European group for numerical weather prediction with participating meteorological services from Germany (DWD, AWGeophys), Greece (HNMS), Italy (USAM, ARPA-SIMC, ARPA Piemonte), Switzerland (MeteoSwiss), Poland (IMGW), Romania (NMA) and Russia (RHM). The general goal is to develop, improve and maintain a non-hydrostatic limited area modelling system to be used for both operational and research applications by the members of COSMO. This system is initially based on the COSMO-Model (previously known as LM) of DWD with its corresponding data assimilation system.

The Technical Reports are intended

- for scientific contributions and a documentation of research activities,
- to present and discuss results obtained from the model system,
- to present and discuss verification results and interpretation methods,
- for a documentation of technical changes to the model system,
- to give an overview of new components of the model system.

The purpose of these reports is to communicate results, changes and progress related to the LM model system relatively fast within the COSMO consortium, and also to inform other NWP groups on our current research activities. In this way the discussion on a specific topic can be stimulated at an early stage. In order to publish a report very soon after the completion of the manuscript, we have decided to omit a thorough reviewing procedure and only a rough check is done by the editors and a third reviewer. We apologize for typographical and other errors or inconsistencies which may still be present.

At present, the Technical Reports are available for download from the COSMO web site (www.cosmo-model.org). If required, the member meteorological centres can produce hard-copies by their own for distribution within their service. All members of the consortium will be informed about new issues by email.

For any comments and questions, please contact the editor:

Massimo Milelli
massimo.milelli@cimafoundation.org